JOURNAL OF PETROLOGY | VOLUME 48 | NUMBER 8 | PAGES 1495–1512 | 2007 | doi:10.1093/petrology/egm027

# The Geochemistry of the Arabian Lithospheric Mantle—a Source for Intraplate Volcanism?

**J. E. SHAW[1,2], J. A. BAKER[1,3], A. J. R. KENT[4], K. M. IBRAHIM[5] AND M. A. MENZIES[2]***

[1]DANISH LITHOSPHERE CENTRE, ØSTER VOLDGADE 10, COPENHAGEN, 1350 K, DENMARK

[2]DEPARTMENT OF GEOLOGY, ROYAL HOLLOWAY UNIVERSITY OF LONDON, EGHAM TW20 0EX, UK

[3]SCHOOL OF EARTH SCIENCES, VICTORIA UNIVERSITY OF WELLINGTON, PO BOX 600, WELLINGTON, NEW ZEALAND

[4]DEPARTMENT OF EARTH SCIENCES, OREGON STATE UNIVERSITY, CORVALLIS, OR97331-5506, USA

[5]DEPARTMENT OF EARTH AND ENVIRONMENTAL SCIENCES, HASHEMITE UNIVERSITY OF JORDAN, ZARQA, JORDAN

**RECEIVED JANUARY 27, 2005; ACCEPTED APRIL 30, 2007**
**ADVANCE ACCESS PUBLICATION JUNE 22, 2007**

*We present trace element and Sr–Nd–Hf–Pb isotope compositions for clinopyroxenes from anhydrous spinel peridotite and garnet ± spinel pyroxenite xenoliths of Pan-African lithospheric mantle from Jordan, including the first high-precision double-spike Pb isotope measurements of mantle clinopyroxene. Clinopyroxenes from the peridotites are variably Th–U–LILE–LREE enriched and display prominent negative Nb, Zr and Ti anomalies. MREE–HREE abundances can generally be modelled as partial melting residues of spinel lherzolite with primitive-mantle-like composition after extraction of 5–10% melt, whereas the enrichments in Th–U–LILE–LREE require a Pan-African or later metasomatic event. The large range of Nd, Sr, Pb and Hf isotope ratios in both peridotites and pyroxenites (e.g.* $\varepsilon Nd \sim 1{\cdot}4$–$17{\cdot}5$; $^{206}Pb/^{204}Pb \sim 17{\cdot}2$–$20{\cdot}4$; $\varepsilon Hf \sim 0{\cdot}6$–$164{\cdot}6$*) encompasses compositions more radiogenic than mid-ocean ridge basalt (MORB), and Pb isotopes cover almost the entire range of oceanic basalt values.* $\varepsilon Hf$ *values are some of the highest ever recorded in mantle samples and are decoupled from* $\varepsilon Nd$ *in the same samples. Marked correlations between Sr–Nd–Pb isotopes, LILE–LREE enrichments and HFSE depletion suggest that the metasomatizing agent was a carbonatitic-rich melt and isotopic data suggest that metasomatism may have been related to Pan-African subduction. The metasomatic melt permeated depleted upper mantle (<16 kbar) during Pan-African subduction at ~600–900 Ma, and the variably metasomatized material was then incorporated into the Arabian lithospheric mantle. There is no evidence for recent metasomatism (<30 Ma) related to the Afar plume like that postulated to have affected southern Arabian lithospheric mantle. Hf isotopes in the mantle clinopyroxenes are unaffected by metasomatism, and even some strongly overprinted lithologies record ancient (>1·2 Ga) pre-metasomatic Lu–Hf signatures of the depleted upper mantle that was the protolith of the Arabian lithospheric mantle. The 'resistance' of the Lu–Hf isotopic system to later metasomatic events resulted in the development of extremely heterogeneous Hf isotopic signatures over time that are decoupled from other isotopic systems. No mantle sample in this study exactly matches the chemical and isotopic signature of the source of Jordanian intraplate basalts. However, the xenolith compositions are broadly similar to those of the source of Arabian intraplate basalts, suggesting that the numerous Cenozoic intraplate volcanic fields throughout Arabia may be the product of melting upper mantle wedge material fertilized during Pan-African subduction and incorporated into the Arabian lithospheric mantle. We propose a model whereby the proto-Arabian lithospheric mantle underwent a major melting event in early Proterozoic–late Archean times (at the earliest at ~1·2 Ga). Island-arc volcanism and major crust formation occurred during the Pan-African orogeny, which liberated fluids and possibly small-degree melts that migrated through the mantle creating zones of enrichment for certain elements depending upon their compatibility. Immobile elements, such as Nb, were concentrated near the base of the mantle wedge providing the source of the Nb-rich Jordanian volcanic rocks. More mobile elements, such as LILE and LREE, were transported up through the mantle and fertilized the shallow mantle source of the Jordanian xenoliths. Following subduction, the mantle wedge became fossilized and preserved distinct enriched and depleted zones. Lithospheric rifting in the Miocene triggered partial melting of spinel-facies mantle in the lower lithosphere, which mixed with deeper asthenospheric garnet-facies melts as rifting evolved. These melts entrained segments of*

*Corresponding author. E-mail: m.menzies@gl.rhul.ac.uk

*variably carbonatite-metasomatized shallow lithospheric mantle* en route *to the surface.*

KEY WORDS: *Arabian lithospheric mantle; Jordan; mantle xenoliths; Sr–Nd–Hf–Pb isotopes*

## INTRODUCTION

Mantle xenoliths transported to the surface in alkali basalts record information about the composition and evolution of the lithospheric mantle. Studies of the composition of ultramafic xenoliths from continental areas suggest that the mantle has undergone a complicated history of depletion and enrichment of various elements. Xenoliths rarely have simple depleted mantle signatures and almost always require some degree of metasomatic enrichment to explain their characteristics (e.g. Menzies *et al.*, 1987; Bodinier *et al.*, 1990; Johnson *et al.*, 1996; Ionov *et al.*, 2002). A variety of metasomatic fluids are commonly called upon to explain trace element patterns, from $H_2O$- and $CO_2$-rich fluids to silicate- and carbonate-rich melts (e.g. Yemen—Baker *et al.*, 1998, 2002). Mantle-derived peridotites displaying enrichment in rare earth elements (REE) without concomitant enrichment in high field strength elements (HFSE) (Ti, Zr, Hf) are common in the geological record and have been interpreted as reflecting chemical interaction with carbonate-rich melts (Hauri *et al.*, 1993). This conclusion is somewhat surprising considering the relative rarity of carbonatitic volcanic rocks on Earth. Furthermore, recent studies (Bedini *et al.*, 1997; Bodinier *et al.*, 2004) have suggested that is not necessary to invoke different and genetically distinct metasomatic melts or fluids (i.e. a hydrous silicate melt and a carbonate melt) as a variety of compositionally different melts, including carbonate-rich ones, can be derived from a single basaltic melt by reactive chromatographic processes.

Mantle xenoliths entrained in late Cenozoic volcanic rocks erupted throughout NW Jordan provide information about the evolution of apparently young (~700 Ma) lithospheric mantle underlying Arabia and could represent a potential source for Arabian intraplate volcanism. Previous chemical and Sr–Nd–Pb isotope studies on Saudi Arabian and Yemen mantle xenoliths (e.g. Henjes-Kunst *et al.*, 1990; Blusztajn *et al.*, 1995; Baker *et al.*, 1998, 2002) have identified a suite of compositionally diverse mantle rocks that represent variably depleted and enriched portions of the Arabian lithosphere. In those studies it was proposed that the formation of the Arabian lithospheric mantle protolith from an already depleted mantle source occurred during accretion and growth of Pan-African crust ~700 Myr ago. The variably enriched xenoliths have been identified as the result of multiple metasomatic overprints, initially by subduction processes associated with Pan-African accretion but also later by small-degree melts from asthenospheric or mantle plume sources. Recent metasomatic events recorded by some Yemen mantle xenoliths have been linked to continental rifting and Afar plume activity that began ~30 Myr ago (Baker *et al.*, 1998).

In this study, we present chemical and Sr–Nd–Hf–Pb isotopic data for clinopyroxenes from 21 mantle-derived peridotites and pyroxenites from the Harrat Ash Shaam volcanic field, Jordan (Fig. 1). Until relatively recently, Lu–Hf and Pb isotopic studies of mantle xenoliths have been hampered by poor analytical precision because of the low concentrations of these elements in mantle rocks, laboratory blank problems (Pb) or difficulties in making the mass spectrometric measurements (Pb and Hf). However, the advent of new analytical methods and improved clean laboratory procedures now allows the acquisition of precise Pb and Hf isotopic data for mantle lithologies, even in samples with $<0{\cdot}1$ and $<0{\cdot}2$ ppm of Pb and Hf, respectively. Herein, we present the first Hf isotopic data on mantle xenoliths from Arabia and the first high-precision Pb isotopic data determined with a Pb double spike on mantle clinopyroxene. With these new data, we identify unusual isotopic signatures and complex trends not observed before in mantle rocks that provide novel insights into ancient depletion and enrichment events in this relatively young example of lithospheric mantle. This information, combined with published studies of the host basalts (Shaw *et al.*, 2003), also allows us to assess the role of the lithospheric mantle in the petrogenesis of Jordanian alkali basalts.

## SAMPLES AND ANALYTICAL TECHNIQUES

### Mantle xenolith classification

The peridotite samples examined in this study are spinel harzburgites and lherzolites and contain a primary assemblage of ol + opx + sp + cpx (<9% modal cpx). One sample (J11) contains partially crystallized melt pockets (~10 modal%) of glass and fine-grained olivine, orthopyroxene and clinopyroxene but there are no accessory phases present in the other samples and, in particular, we did not identify amphibole in any of these or the much larger suite of Jordanian xenoliths from which these samples were selected. Jordanian pyroxenites encompass a wide range of compositions, including garnet, spinel and plagioclase websterites. Xenoliths of similar composition have been reported in Jordan, Syria and Saudi Arabia (Kuo & Essene, 1986; McGuire, 1988a, 1988b; Nasir & Al-Fuqha, 1988; Blusztajn *et al.*, 1995; Nasir & Safarjalani, 2000).

Previous work on Jordanian mantle xenoliths (Nasir, 1992) reported temperatures and pressures of 900–1030°C and 12–18 kbar (37–60 km) and 940–1020°C and 11–13 kbar (35–43 km) for peridotites and pyroxenites, respectively. The lower end of this range is close to

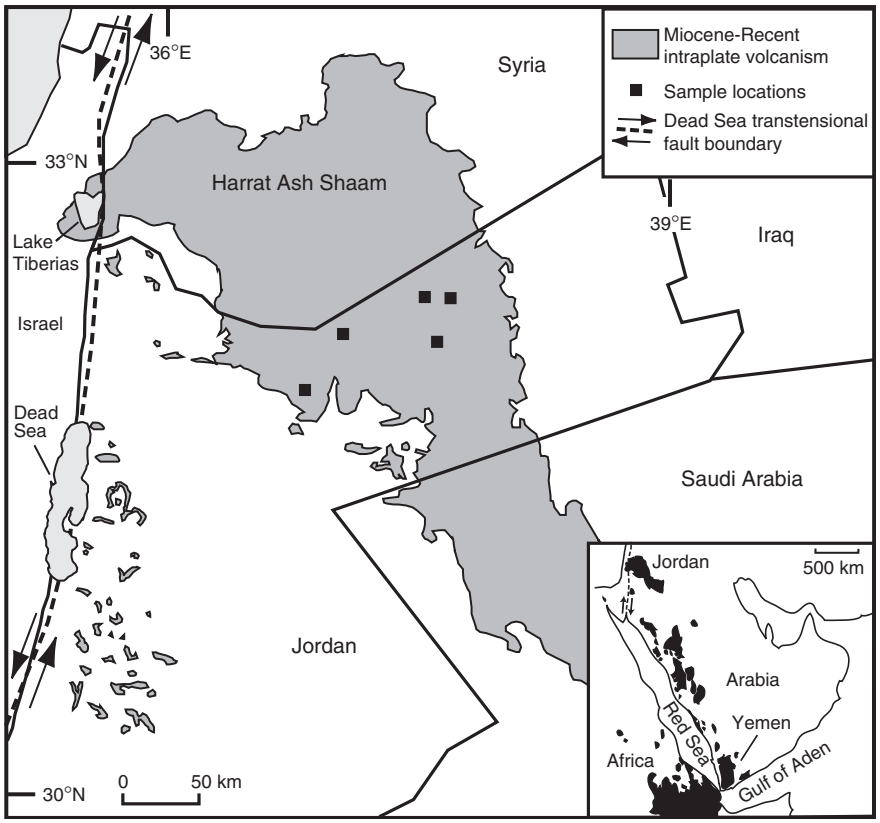


**Fig. 1.** Map of volcanism in northwestern Arabia, showing the extent of Miocene–Recent intraplate volcanism in Jordan and the locations of the mantle xenolith samples analysed in this study. Inset: regional map of the Afro-Arabian area.

estimates for the crust–mantle boundary (~35–37 km) (El Isa *et al.*, 1987; Nasir, 1992, 1995). Xenolith studies in Saudi Arabia yield similar temperature and pressure conditions for peridotites (900–980°C and 13–19 kbar) and pyroxenites (1000–1070°C and 13·8–16·5 kbar) (McGuire, 1988*a*) and support a shallow lithospheric mantle origin for both the Jordanian and Saudi Arabian xenoliths.

## Analytical procedures

Clinopyroxene Lu–Hf–U–Th–Pb abundances determined by isotope dilution and Sr–Nd–Hf–Pb isotopic analyses are presented in Table 1. Major and trace element data for most of these samples are given in Table 2. All chemical and isotopic analyses were performed on clinopyroxene separates as this phase is the dominant host of incompatible trace elements in mantle rocks. Mineral separates were carefully handpicked under a binocular microscope, rinsed in distilled water and dried in an oven prior to leaching and chemical digestion.

Major element compositions were determined by electron microprobe at the Geological Institute, University of Copenhagen. Most trace element abundances were determined by laser-ablation inductively coupled plasma mass spectrometry (ICP-MS) at Oregon State University under conditions similar to those reported in Kent *et al.* (2004). Ablation was carried out using He as the carrier gas, and this was mixed with Ar immediately prior to the plasma torch. Background count rates were measured for 30 s before ablation commenced for each analysis. Plasma torch conditions were optimized so that ThO/Th ratios were $<2\%$. Analyses were performed in spot mode—using a stationary laser to progressively ablate a crater in the sample materials. Each individual analysis represents 40 s data acquisition during ablation using an 80 μm spot and with pulse frequency of 4 Hz, resulting in an ablation crater ~15 μm deep. Trace element abundances were calculated relative to the USGS glass standard BCR-2G, which was analysed under identical conditions throughout the analysis session [see Kent *et al.* (2004) for the elements used for calibration]. $^{43}$Ca was used as the internal normalizing isotope in conjunction with CaO contents measured by electron microprobe.

For Sr–Nd–Hf–Pb isotopic analysis, clinopyroxenes were acid-leached in 6M HCl for 1 h at 120°C prior to digestion. Sr and Nd isotope ratios were determined by thermal ionization mass spectrometry (TIMS) at Royal Holloway University of London (RHUL) (Thirlwall, 1991*a*, 1991*b*). Internal precision for $^{87}Sr/^{86}Sr$ was $\leq \pm 0{\cdot}000013$ (2 SE)

*Table 1: Lu–Hf–U–Th–Pb isotope dilution trace element data and Sr–Nd–Hf–Pb isotope ratios of clinopyroxene in Jordanian mantle xenoliths*

| Sample no. | Rock | $^{87}Sr/^{86}Sr$ | $^{143}Nd/^{144}Nd$ | εNd | U (ppm) | Th (ppm) | Pb (ppm) | $^{206}Pb/^{204}Pb$ | $^{207}Pb/^{204}Pb$ | $^{208}Pb/^{204}Pb$ | △7/4 | △8/4 | Lu (ppm) | Hf (ppm) | $^{176}Lu/^{177}Hf$ | $^{176}Hf/^{177}Hf$ | εHf | △εHf |
|---|---|---|---|---|---|---|---|---|---|---|---|---|---|---|---|---|---|---|
| J8 | pd | 0·70303 | 0·513136 | 9·7 | | | | 18·5011 ± 79† | 15·5511 ± 67 | 38·3000 ± 162 | 5·5 | 30·5 | 0·2455 | 0·5087 | 0·0685 | 0·283660 ± 53 | 31·4 | 15·1 |
| J8 dup | pd | | | | | | | 18·5942 ± 69 | 15·5598 ± 60 | 38·3585 ± 145 | 5·3 | 25·1 | 0·2372 | 0·5164 | 0·0652 | 0·283695 ± 6 | 32·6 | 16·3 |
| J10 | pd | 0·70298 | 0·512856 | 4·3 | 0·2321 | 0·7722 | 0·8869 | 20·12862 ± 14 | 15·6926 ± 13 | 39·7443 ± 41 | 2·0 | −21·8 | 0·1394 | 0·6826 | 0·0290 | 0·283105 ± 29 | 11·8 | 2·9 |
| J10 dup | pd | | | | | | | 20·1420 ± 12 | 15·6913 ± 11 | 39·7526 ± 32 | 1·7 | −22·6 | 0·1395 | 0·7226 | 0·0274 | 0·283095 ± 6 | 11·4 | 2·5 |
| J11 | pd | 0·70302 | 0·512848 | 4·1 | 0·2060 | 0·7099 | 0·4035 | 20·3610 ± 22 | 15·7105 ± 19 | 40·0378 ± 56 | 1·2 | −20·6 | 0·1655 | 0·1361 | 0·1726 | 0·287425 ± 26 | 164·6 | 155·9 |
| J11 dup | pd | | | | | | | 20·3758 ± 15 | 15·7125 ± 14 | 40·0733 ± 37 | 1·3 | −18·8 | 0·1656 | 0·1361 | 0·1728 | 0·287507 ± 17 | 167·4 | 158·7 |
| J12 | pd | 0·70308 | 0·512825 | 3·6 | 0·1343 | 0·4060 | 0·1591 | 19·8900 ± 26 | 15·6680 ± 21 | 39·5892 ± 58 | 2·1 | −8·5 | 0·1359 | 0·8351 | 0·0231 | 0·282838 ± 23 | 2·3 | −5·7 |
| J12 dup | pd | | | | | | | 19·8972 ± 24 | 15·66567 ± 21 | 39·5896 ± 52 | 1·8 | −9·3 | 0·1312 | 0·8509 | 0·0219 | 0·282790 ± 5 | 0·6 | −7·5 |
| KKJ004 | pd | | | | | | | 19·5211 ± 20 | 15·6448 ± 16 | 39·1010 ± 42 | 3·8 | −12·7 | | | | | | |
| KKJ007 | px | 0·70282 | 0·513006 | 7·2 | | | | 18·6484 ± 15 | 15·5067 ± 14 | 38·3546 ± 38 | −0·6 | 18·2 | 0·0502 | 1·1132 | 0·0064 | 0·282940 ± 4 | 5·9 | −7·0 |
| KKJ0037 | px | 0·70276 | 0·513039 | 7·8 | 0·0043 | 0·0095 | 0·0605 | 18·3883 ± 44 | 15·5234 ± 39 | 38·2390 ± 96 | 3·9 | 38·1 | 0·0379 | 0·5011 | 0·0107 | 0·283188 ± 6 | 14·7 | 0·9 |
| KKJ0046 | px | 0·70250 | 0·513307 | 13·1 | | | | 19·0067 ± 29 | 15·5745 ± 25 | 38·7640 ± 62 | 2·3 | 15·8 | 0·1000 | 0·2827 | 0·0502 | 0·283339 ± 66 | 20·1 | −0·8 |
| KKJ0046 dup | px | | | | | | | | | | | | 0·1118 | 0·2905 | 0·0547 | 0·283318 ± 11 | 19·3 | −1·6 |
| KKJ0058 | pd | | | | | | | 18·8460 ± 62 | 15·6127 ± 46 | 38·5033 ± 132 | 7·9 | 9·2 | | | | | | |
| KKJ0063 | pd | 0·70342 | 0·512710 | 1·4 | 0·1123 | 0·2808 | 0·2953 | 20·1881 ± 12 | 15·6711 ± 11 | 40·3096 ± 31 | −0·8 | 27·5 | 0·1692 | 0·4428 | 0·0542 | 0·283412 ± 7 | 22·6 | 17·6 |
| KKJ0063 dup | pd | | | | | | | 20·1930 ± 18 | 15·6661 ± 16 | 40·3092 ± 45 | −1·4 | 26·9 | | | | | | |
| KKJ0064 | pd | 0·70303 | 0·513536 | 17·5 | 0·0137 | 0·0182 | 0·1139 | 18·1508 ± 41 | 15·5241 ± 38 | 38·0669 ± 94 | 6·6 | 49·6 | 0·2195 | 0·2821 | 0·1105 | 0·285445 ± 11 | 94·5 | 67·6 |
| KKJ0064 dup | pd | | | | | | | 18·1466 ± 35 | 15·5185 ± 31 | 38·0459 ± 78 | 6·0 | 48·0 | | | | | | |
| KKJ0065 | pd | 0·70278 | 0·513108 | 9·2 | 0·2314 | 0·7049 | 0·7455 | 19·1162 ± 14 | 15·5811 ± 13 | 38·8225 ± 34 | 1·8 | 8·4 | 0·2743 | 0·7160 | 0·0544 | 0·283440 ± 5 | 23·6 | 8·0 |
| KKJ0065 dup | pd | | | | | | | 19·1291 ± 16 | 15·5830 ± 15 | 38·8385 ± 37 | 1·8 | 8·4 | | | | | | |
| KKJ0070 | pd | 0·70225 | 0·513401 | 14·9 | 0·0024 | | 0·0607 | 18·0160 ± 63 | 15·4525 ± 60 | 37·4805 ± 145 | 0·9 | 7·2 | 0·1978 | 0·5085 | 0·0552 | 0·283313 ± 24 | 19·1 | −4·2 |
| KKJ0070 dup | pd | | | | | | | 17·9371 ± 61 | 15·4479 ± 55 | 37·4129 ± 133 | 1·3 | 10·0 | 0·2639 | 0·6356 | 0·0589 | 0·283318 ± 11 | 19·3 | −4·1 |
| KKJ0070 dup | pd | | | | | | | 18·0080 ± 31 | 15·4535 ± 30 | 37·4732 ± 73 | 1·0 | 7·5 | | | | | | |
| KKJ0071 | px | | | | | | | | | | | | | | | 0·284743 ± 50 | 69·7 | |
| KKJ0073 | px | | | | | | | 19·3388 ± 17 | 15·6147 ± 15 | 38·5483 ± 35 | 2·7 | −45·9 | | | | | | |
| KKJ0075 | pd | 0·70282 | 0·513073 | 8·5 | | | | 19·2365 ± 12 | 15·6002 ± 29 | 38·9615 ± 73 | 2·4 | 7·8 | 0·2590 | 0·8795 | 0·0418 | 0·283396 ± 22 | 22·1 | 7·4 |
| KKJ0075 dup | pd | | | | | | | 19·2665 ± 44 | 15·6032 ± 34 | 38·9867 ± 90 | 2·4 | 6·6 | 0·2417 | 0·8238 | 0·0417 | 0·283363 ± 28 | 20·9 | 6·2 |
| KKJ0080 | pd | | | | | | | 17·1684 ± 78 | 15·3755 ± 56 | 36·6049 ± 168 | 2·3 | 22·1 | | | | | | |
| KKJ0082 | pd | | | | | | | 19·2507 ± 34 | 15·6160 ± 27 | 38·8872 ± 70 | 3·8 | −1·4 | | | | | | |
| KKJ0084 | pd | 0·70245 | 0·513460 | 16·0 | 0·0893 | 0·2167 | 0·2618 | 19·9954 ± 16 | 15·6545 ± 14 | 39·7150 ± 39 | −0·4 | −8·6 | 0·2602 | 0·7726 | 0·0478 | 0·283470 ± 30 | 24·7 | −0·3 |
| KKJ0084 dup | pd | | | | | | | 19·9981 ± 21 | 15·6553 ± 19 | 39·7191 ± 50 | −0·4 | −8·6 | 0·2657 | 0·7017 | 0·0538 | 0·283459 ± 7 | 24·3 | −0·6 |
| KKJ0089 | pd | 0·70265 | 0·513163 | 10·2 | | | | 19·5907 ± 18 | 15·6233 ± 14 | 39·4486 ± 40 | 0·9 | 13·6 | 0·2526 | 0·6630 | 0·0541 | 0·283391 ± 36 | 21·9 | 4·8 |
| KKJ0089 dup | pd | | | | | | | 19·5710 ± 20 | 15·5985 ± 17 | 39·3682 ± 44 | −1·4 | 8·0 | 0·2556 | 0·5770 | 0·0629 | 0·283309 ± 8 | 19·0 | 1·9 |
| KKJ0090 | pd | 0·70272 | 0·513276 | 12·4 | 0·1818 | 0·6306 | 0·3954 | 19·4120 ± 10 | 15·6378 ± 9 | 39·1149 ± 22 | 4·3 | 1·9 | 0·2333 | 0·7360 | 0·0450 | 0·283616 ± 31 | 29·8 | 9·8 |
| KKJ0090 dup | pd | | | | | | | 19·4284 ± 13 | 15·6264 ± 12 | 39·0951 ± 34 | 2·9 | −2·1 | 0·2099 | 0·5971 | 0·0499 | 0·283550 ± 7 | 27·5 | 7·5 |

pd, peridotite; px, pyroxenite; dup, duplicate. △7/4 and △8/4 are from Hart (1984).
*△εHf = εHf − (1·36εNd + 3·13) (Nowell *et al.*, 1998).
†Errors are 2 SE internal precision.

*Table 2: Clinopyroxene major and trace element data for selected Jordanian mantle xenoliths*

| Sample no.: | J8 | J10 | J11 | J12 | KKJ0037 | KKJ0046 | KKJ0063 | KKJ0064 | KKJ0065 | KKJ0070 | KKJ0075 | KKJ0084 | KKJ0089 | KKJ0090 |
|---|---|---|---|---|---|---|---|---|---|---|---|---|---|---|
| Rock: | pd | pd | pd | pd | px | px | pd | pd | pd | pd | pd | pd | pd | pd |
| *wt %* | | | | | | | | | | | | | | |
| $SiO_2$ | 52·31 | 53·07 | 52·96 | 52·52 | 50·67 | 50·77 | 52·38 | 52·08 | 52·13 | 50·79 | 51·56 | 51·99 | 51·90 | 52·12 |
| $Al_2O_3$ | 5·39 | 4·27 | 4·50 | 4·52 | 7·05 | 7·40 | 4·21 | 5·74 | 6·02 | 7·82 | 6·61 | 5·69 | 5·79 | 5·64 |
| FeO | 2·13 | 2·51 | 2·24 | 2·46 | 3·02 | 2·61 | 2·37 | 1·91 | 2·57 | 2·59 | 2·75 | 2·73 | 2·56 | 2·31 |
| MgO | 15·03 | 15·66 | 15·58 | 15·92 | 14·49 | 13·80 | 15·29 | 14·74 | 15·66 | 14·94 | 15·15 | 15·29 | 15·14 | 15·06 |
| CaO | 21·45 | 20·62 | 20·90 | 21·18 | 20·93 | 21·56 | 21·22 | 20·69 | 19·32 | 20·01 | 19·51 | 20·40 | 20·58 | 20·67 |
| $K_2O$ | 0·01 | 0·01 | b.d.2 | 0·01 | 0·01 | 0·01 | 0·01 | 0·01 | b.d. | 0·01 | 0·01 | b.d. | 0·01 | 0·01 |
| $Na_2O$ | 1·44 | 1·61 | 1·51 | 1·24 | 1·19 | 1·39 | 1·41 | 1·94 | 1·80 | 1·72 | 1·72 | 1·67 | 1·62 | 1·74 |
| $TiO_2$ | 0·35 | 0·19 | 0·12 | 0·49 | 0·43 | 0·23 | 0·28 | 0·23 | 0·42 | 0·51 | 0·45 | 0·44 | 0·49 | 0·49 |
| MnO | 0·08 | 0·07 | 0·07 | 0·06 | 0·09 | 0·06 | 0·07 | 0·08 | 0·09 | 0·10 | 0·12 | 0·08 | 0·10 | 0·08 |
| NiO | 0·04 | 0·06 | 0·02 | 0·06 | 0·04 | 0·02 | 0·04 | 0·03 | 0·05 | 0·06 | 0·06 | 0·05 | 0·04 | 0·04 |
| $Cr_2O_3$ | 0·82 | 1·22 | 1·03 | 0·97 | 0·71 | 0·10 | 0·99 | 1·18 | 0·87 | 0·96 | 0·77 | 0·71 | 0·68 | 0·97 |
| Cl | 0·01 | 0·01 | b.d. | b.d. | b.d. | b.d. | 0·01 | 0·01 | b.d. | b.d. | b.d. | b.d. | 0·01 | 0·01 |
| Total | 99·06 | 99·30 | 98·93 | 99·42 | 98·64 | 97·96 | 98·28 | 98·64 | 98·93 | 99·52 | 98·70 | 99·08 | 98·93 | 99·15 |
| mg-no. | 0·93 | 0·92 | 0·93 | 0·92 | 0·90 | 0·90 | 0·92 | 0·93 | 0·92 | 0·91 | 0·91 | 0·91 | 0·91 | 0·92 |
| *ppm* | | | | | | | | | | | | | | |
| Co | 22 | 26 | 23 | 26 | 22 | 18 | 14 | 15 | 16 | 16 | 21 | 17 | 17 | 16 |
| V | 302 | 368 | 290 | 336 | 238 | 178 | 242 | 227 | 234 | 223 | 229 | 226 | 224 | 240 |
| Sc | 71 | 94 | 82 | 80 | 27 | 34 | 73 | 52 | 51 | 56 | 50 | 55 | 52 | 50 |
| Pb | b.d. | 1·1 | 0·5 | 0·2 | 0·1 | 0·1 | 0·7 | 0·1 | 0·3 | b.d. | 0·1 | 0·2 | 0·2 | 0·3 |
| Sr | 29·2 | 212·3 | 156·8 | 107·7 | 29·9 | 33·8 | 45·3 | 16·2 | 74·1 | 22·0 | 108·8 | 33·5 | 38·5 | 55·1 |
| Rb | b.d. | b.d. | 0·10 | 0·38 | b.d. | 0·04 | b.d. | 0·09 | b.d. | 0·03 | 0·03 | 0·03 | 0·06 | 0·03 |
| Ba | 1·12 | 0·17 | 0·49 | 0·28 | 0·27 | 0·13 | 0·10 | 0·94 | 0·11 | b.d. | 0·20 | 0·14 | 0·25 | 0·25 |
| Zr | 8·7 | 20·5 | 2·9 | 17·4 | 6·9 | 4·4 | 9·7 | 3·5 | 9·9 | 10·0 | 16·9 | 11·4 | 8·2 | 10·8 |
| Hf | 0·52 | 0·72 | 0·14 | 0·85 | 0·50 | 0·29 | 0·44 | 0·28 | 0·72 | 0·64 | 0·82 | 0·70 | 0·58 | 0·60 |
| Nb | 0·20 | 0·70 | 0·53 | 1·12 | 0·09 | 0·07 | 0·27 | 0·05 | 0·04 | 0·01 | 0·86 | 0·09 | 0·21 | 0·07 |
| Th | 0·01 | 0·77 | 0·76 | 0·42 | 0·01 | 0·03 | 0·76 | b.d. | 0·36 | b.d. | 0·48 | 0·18 | 0·26 | 0·42 |
| U | 0·02 | 0·32 | 0·29 | 0·20 | b.d. | 0·01 | 0·29 | 0·01 | 0·14 | 0·01 | 0·17 | 0·10 | 0·09 | 0·20 |
| Y | 10·2 | 8·5 | 7·1 | 8·7 | 2·8 | 3·4 | 5·4 | 7·4 | 9·4 | 11·5 | 10·7 | 10·4 | 9·8 | 9·3 |
| La | 0·57 | 11·24 | 10·27 | 3·99 | 0·62 | 0·37 | 4·85 | 0·12 | 3·26 | 0·09 | 5·37 | 1·25 | 2·54 | 2·50 |
| Ce | 2·33 | 33·18 | 25·73 | 9·80 | 2·63 | 0·91 | 9·46 | 0·49 | 9·20 | 0·81 | 13·15 | 1·64 | 4·82 | 4·74 |
| Pr | 0·40 | 3·74 | 2·53 | 1·27 | 0·44 | 0·13 | 0·98 | 0·09 | 1·02 | 0·23 | 1·53 | 0·32 | 0·55 | 0·54 |
| Nd | 2·23 | 13·30 | 7·84 | 6·07 | 2·41 | 0·71 | 3·63 | 0·67 | 3·71 | 1·79 | 5·98 | 2·16 | 2·66 | 2·80 |
| Sm | 0·92 | 2·50 | 1·15 | 2·01 | 0·78 | 0·36 | 0·81 | 0·45 | 1·04 | 0·95 | 1·53 | 1·02 | 1·09 | 1·12 |
| Eu | 0·41 | 0·89 | 0·44 | 0·83 | 0·35 | 0·24 | 0·35 | 0·24 | 0·48 | 0·47 | 0·64 | 0·48 | 0·51 | 0·54 |
| Gd | 1·3 | 2·0 | 1·1 | 2·3 | 1·0 | 0·7 | 0·8 | 0·9 | 1·4 | 1·6 | 1·8 | 1·6 | 1·7 | 1·7 |
| Dy | 1·9 | 1·9 | 1·3 | 2·2 | 0·9 | 0·8 | 1·1 | 1·5 | 1·8 | 2·3 | 2·1 | 2·2 | 2·1 | 2·1 |
| Er | 1·26 | 0·97 | 0·94 | 1·07 | 0·32 | 0·36 | 0·78 | 1·01 | 1·19 | 1·45 | 1·26 | 1·41 | 1·37 | 1·37 |
| Yb | 1·3 | 0·9 | 1·0 | 0·9 | 0·1 | 0·3 | 0·8 | 1·0 | 1·1 | 1·4 | 1·2 | 1·3 | 1·3 | 1·2 |
| Lu | 0·24 | 0·14 | 0·17 | 0·13 | 0·04 | 0·11 | 0·17 | 0·22 | 0·27 | 0·26 | 0·24 | 0·27 | 0·26 | 0·21 |

pd, peridotite; px, pyroxenite; b.d., below detection limit.

for all but one sample (±0·000044) and ≤±0·000005 for $^{143}Nd/^{144}Nd$. External reproducibility for $^{87}Sr/^{86}Sr$ and $^{143}Nd/^{144}Nd$ is ±0·000014 ($n = 348$, 2 SD) and ±0·000007 ($n = 68$, 2 SD), respectively. $^{87}Sr/^{86}Sr$ is reported relative to a value of 0·710248 for SRM 987 and $^{143}Nd/^{144}Nd$ is reported relative to 0·511418 for a dilute Aldrich standard. Procedural blanks were 2·4 ng and 0·18 ng for Sr and Nd, respectively, and are insignificant.

U–Th–Pb ID and Pb–Lu–Hf isotopic analyses were performed on an Axiom multiple-collector ICP-MS system at the Danish Lithosphere Centre (DLC), Copenhagen. Given that Lu–Hf and precise Pb isotopic analysis of mantle samples are relatively novel methods we describe in some detail the techniques used for this work and results of replicate analyses of the same samples, including acid-leaching experiments prior to Pb isotopic analysis. Chemical separation and mass spectrometry procedures for Lu and Hf follow those described by Ulfbeck *et al.* (2002) and Bizzarro *et al.* (2003). Procedural blanks during this study were ~50 pg for Hf and <2 pg for Lu and are insignificant. In general, replicate digestions of each sample were undertaken, the first primarily designed to obtain Lu–Hf isotope dilution (ID) concentration measurements that would permit proper spiking for later analyses. Given constraints on the amounts of sample material available, only a small amount of material was digested in the first series of analyses, and thus relatively poor internal precision was obtained (±0·000022 to 0·000066) (2 SE) for $^{176}Hf/^{177}Hf$ (excluding J11; ±0·000264). Internal precision for $^{176}Hf/^{177}Hf$ (2 SE) during the second round of analyses on larger mineral separates (50–100 mg) was significantly improved (±0·000004 to 0·000028). Out of 10 replicate analyses seven reproduce within internal precision of the replicate analyses. Three replicate analyses show a slight discrepancy (up to 2·5 εHf units) between the different sets of analyses, but given these discrepancies are less than the external reproducibility that we estimate for our method based on repeated analysis of standards (i.e. two times internal precision) we do not regard these differences as being significant. In all cases, interferences from Yb and Lu were reduced to insignificant levels by the chemical separation procedure. External reproducibility for $^{176}Hf/^{177}Hf$ was <±0·000010 for an in-house standard and all Hf isotope data are reported relative to a value of 0·28216 for international standard JMC 475. Based on analysis of dilute solutions of our in-house standard we estimate the external reproducibility of lower precision analyses of low-Hf clinopyroxenes to be approximately two times the internal precision. Reproducibility of $^{176}Lu/^{177}Hf$ estimated from repeated analysis of international basalt standard BHVO-1 yielded a reproducibility of ±0·2%, similar to that obtained on a synthetic mixed Lu–Hf Ames metal solution (±0·15%) (Bizzarro *et al.*, 2003). However, it is evident from Table 1 that replicate Lu/Hf analyses of the mantle clinopyroxenes reproduce to between 0·1 and 10%, with both Lu and Hf concentrations showing variability significantly larger than that expected from analytical errors, although replicate $^{176}Hf/^{177}Hf$ ratios are generally in good agreement. Although further work is required to establish the cause of this variability, we consider that it is probably related to sample heterogeneity and/or irreproducible acid-leaching of the mineral separates prior to digestion.

Samples for U, Th and Pb isotope dilution analysis were spiked with a $^{204}Pb$ and combined $^{229}Th$–$^{236}U$ spike. Column procedures for U–Th were similar to those described by Turner *et al.* (1996). Data were normalized for mass bias by comparison with repeated analysis of SRMU112a. The analytical procedures for Pb have been detailed by Baker *et al.* (2004). Internal precision for $^{206}Pb/^{204}Pb$, $^{207}Pb/^{204}Pb$ and $^{208}Pb/^{204}Pb$ was better than ±0·0035, ±0·0040 and ±0·0070 (2 SE) for the majority of samples. Despite the fact that replicate digestions of basaltic rocks samples using this method reproduce to <± 100 ppm, comparable with reproducibility of the Pb standard SRM981 (Baker *et al.*, 2004), only three of the 12 replicate analyses reproduced within error (KKJ0064, KKJ0070 and KKJ0084). The rest of the samples produced deviations from 240 to 5050 ppm for $^{206}Pb/^{204}Pb$ and from <100 to 1500 ppm for $^{207}Pb/^{204}Pb$. Given the failure of Pb isotopic analyses of replicate digestions to repeat within double-spike errors, even considering the relatively large internal precision obtained on some analyses, we carried out a step leaching experiment on one sample to ascertain what might be responsible for the observed variability, the results of which are described in the next section. Pb is reported relative to $^{206}Pb/^{204}Pb = 16·9412$, $^{207}Pb/^{204}Pb = 15·4990$ and $^{208}Pb/^{204}Pb = 36·7215$ for SRM 981 and external reproducibility obtained on the standard is ± 0·0011, ±0·0011 and ± 0·0031 (2 SD) ($n = 95$) for $^{206}Pb/^{204}Pb$, $^{207}Pb/^{204}Pb$ and $^{208}Pb/^{204}Pb$, respectively (Baker *et al.*, 2004). Procedural blanks were 5–10 pg and insignificant even considering the small amounts of Pb in the clinopyroxene.

### *Pb step leaching experiment*

An acid step leaching experiment was carried out on sample J11 to determine what strength of acid and leaching time are adequate to remove extraneous Pb, for example, from contamination during sample handling, surficial weathering or interaction with the host magmas during ascent to the surface. Clinopyroxene was progressively leached using variable acid types, acid strengths, durations and temperatures, and the leachate from each step was collected, processed to separate Pb, and analysed for Pb isotopes. The sequential leaching steps were as follows: (A) cold 2M HCl for 5 min; (B) cold 2M HCl whilst being ultrasonically agitated for 1 h; (C) cold 6M HCl whilst being ultrasonically agitated for 1 h; (D) hot 6M HCl for 1 h; (E) hot concentrated HF–$HNO_3$ for 3 h; (F) hot HF–$HNO_3$ for 36 h; (G) hot HF–$HNO_3$ for 36 h on the residue from step F (in turn collected after step E); (R) the remaining residue (collected after step G). Pb isotopes were then measured on the leachates and corrected for instrumental mass bias using a $^{207}Pb$–$^{204}Pb$

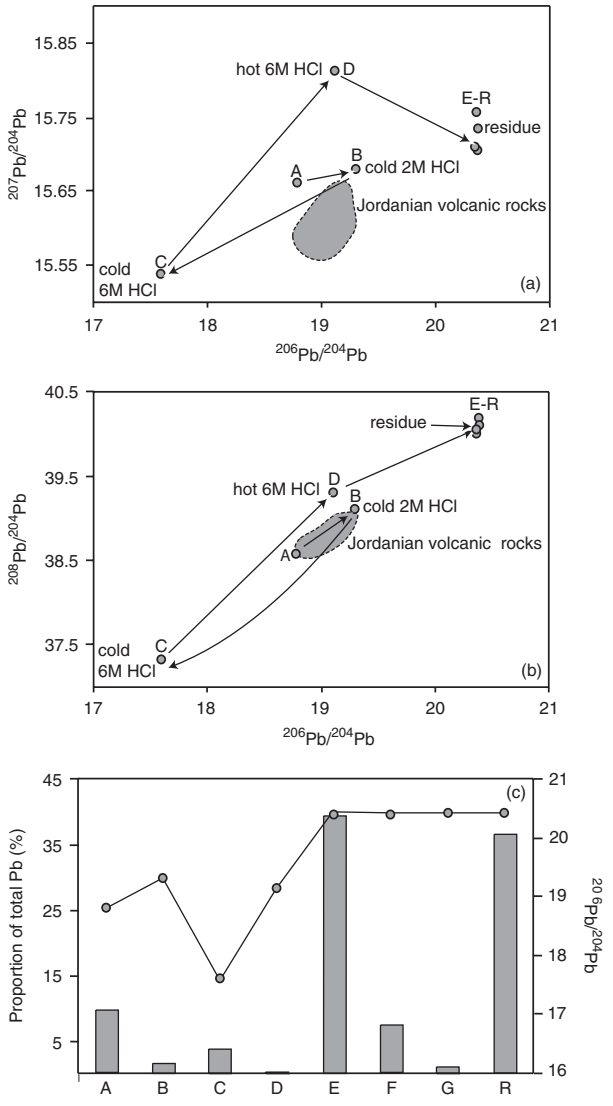


**Fig. 2.** Results of the step leaching experiment for mantle xenolith J11. In (c), the grey bars indicate the percentage of Pb in each leachate on the primary *y*-axis as listed in Table 2 and the line indicates the $^{206}Pb/^{204}Pb$ composition of each leachate on the secondary *y*-axis.

double spike method as described by Baker *et al.* (2004). The results are illustrated in Fig. 2a–c and listed in Table 3.

Pb isotope ratios on both the 2M HCl acid leaches (steps A and B) are similar to data for Cenozoic Jordanian intraplate basalts. This may reflect removal of basalt glass on the surface of the clinopyroxenes incorporated into the xenoliths *en route* to the surface, and emphasizes the importance of the leaching process to reveal accurate mantle signatures. Leachate C has an unradiogenic $^{206}Pb/^{204}Pb$ ratio of 17·6 and a $^{206}Pb/^{207}Pb$ ratios of 1·132, similar to anthropogenic lead ($^{206}Pb/^{207}Pb \sim 1{\cdot}158$) (Véron *et al.*, 1994). All the other leachates in this study have $^{206}Pb/^{207}Pb$ ratios >1·2. If leachate C does represent anthropogenic lead, it is surprising this signature was not removed immediately in the initial 2M HCl leaches of steps A and B. Alternatively, leachate C may represent the dissolution of inclusions soluble in 6M HCl; for example, sulphide inclusions that have low U/Pb and Th/Pb. The subsequent hot 6M HCl leach (D) has a $^{206}Pb/^{204}Pb$ and $^{208}Pb/^{204}Pb$ signature that is more comparable with leachates A and B but has significantly higher $^{207}Pb/^{204}Pb$. However, the data for leachate D exhibit large errors, which are due to a very small Pb contribution from this step (0·16%). Taking this into account, leachate D probably represents an average of the low μ component and the real mantle value. The various HCl acid leachates comprise about 15% of the total Pb released from the digestion of J11 clinopyroxene, with most of the extraneous Pb being readily removable in cold 2M or 6M HCl after only a few minutes.

The remaining leachates show much less variability and approach the clinopyroxene Pb isotopic composition. Leachates E and F are within error of one another but are marginally less radiogenic than R (leachate G had too little Pb to permit a precise analysis). It appears that over one-third of the clinopyroxene-hosted Pb is released by 3 h of digestion in $HF + HNO_3$ and little more is dissolved by repeated $HF + HNO_3$ digestion. Two replicate digestions of J11 clinopyroxene carried out independently of the step leaching experiment (Table 1), after leaching for 1 h in hot 6M HCl, are very similar to analyses of leachate steps E and F, although one of the digestions shows greater variability than permitted by analytical errors alone. Interestingly, the final residue from the step leaching experiment has a Pb isotopic composition that diverges slightly from all the other HF-based digestions. This analysis lies at slightly elevated Pb isotope ratios along a mass fractionation trajectory through the other analyses. Whereas intra-mineral heterogeneity with this variability cannot be excluded as the cause of the variation, it is indeed possible that our extensive acid leaching during the step leaching experiment has induced fractionation of the Pb isotopes of *c.* 1500 ppm per atomic mass unit (a.m.u.).

In summary and by way of recommendation, our leaching experiment has shown the following. (1) Significant extraneous Pb needs to be removed from the mantle clinopyroxenes to obtain the mantle Pb isotopic signature. Given the amount of extraneous Pb associated with J11, some lower Pb samples will be almost totally dominated by this extraneous Pb (*c.* 90%) prior to leaching. (2) The extraneous Pb may be sourced from the host basalts, anthropogenic contamination of the xenoliths on the surface or during separation of mineral separates, the presence of readily soluble low U/Pb and Th/Pb inclusions, or a combination of these processes. (3) Leaching in hot 6M HCl removes nearly all of the extraneous Pb. However, despite the fact that these leaching procedures were

*Table 3: Pb isotope ratios from the step leaching experiment (J11)*

| Sample | $^{206}Pb/^{204}Pb$ | $^{207}Pb/^{204}Pb$ | $^{208}Pb/^{204}Pb$ | Amount Pb% | Weighted averages | | |
|---|---|---|---|---|---|---|---|
| | | | | | $^{206}Pb/^{204}Pb$ | $^{207}Pb/^{204}Pb$ | $^{208}Pb/^{204}Pb$ |
| J11-A | 18·776 ± 2* | 15·661 ± 2 | 38·612 ± 5 | 9·82 | 20·102 | 15·708 | 39·818 |
| J11-B | 19·296 ± 18 | 15·680 ± 14 | 39·132 ± 37 | 1·63 | 20·246 | 15·713 | 39·949 |
| J11-C | 17·595 ± 5 | 15·537 ± 5 | 37·306 ± 11 | 3·66 | 20·264 | 15·714 | 39·964 |
| J11-D | 19·116 ± 108 | 15·812 ± 99 | 39·320 ± 254 | 0·16 | 20·379 | 15·721 | 40·078 |
| J11-E | 20·372 ± 1 | 15·711 ± 1 | 40·045 ± 2 | 39·51 | 20·381 | 15·721 | 40·080 |
| J11-F | 20·368 ± 3 | 15·709 ± 3 | 40·041 ± 6 | 7·53 | 20·389 | 15·730 | 40·110 |
| J11-G | 20·381 ± 19 | 15·752 ± 16 | 40·162 ± 42 | 1·00 | 20·393 | 15·734 | 40·124 |
| J11-R | 20·393 ± 1 | 15·733 ± 1 | 40·123 ± 2 | 36·69 | 20·393 | 15·733 | 40·123 |

*Errors are 2 SE internal precision.
The details of each leaching stage are outlined in the text. The weighted averages represent the remaining bulk sample after each leaching step.

adopted prior to digestion for all the samples listed in Table 1, only *c.* 25% of the samples reproduce within assigned uncertainties. Given that most replicate analyses involve relatively large discrepancies in $^{206}Pb/^{204}Pb$ and $^{208}Pb/^{204}Pb$ but not $^{207}Pb/^{204}Pb$, irreproducible leaching of the clinopyroxene separates probably controls the reproducibility of replicate digestions, although we cannot preclude the possibility that some real inter-crystal trace element heterogeneity of U, Th and Pb (as observed from laser ablation data; not shown) is responsible for the isotopic heterogeneity of replicate digestions. Nevertheless, in conclusion we point out that an average difference of 380 ppm (or ±0·003 from the mean ratio) on the $^{207}Pb/^{204}Pb$ ratio of replicate digestions represents a level of reproducibility not previously attained for Pb isotope studies of mantle xenoliths.

# RESULTS

## Trace element chemistry of clinopyroxenes

Two types of peridotites are identified in our sample suite on the basis of clinopyroxene light REE to heavy REE (LREE/HREE) ratios, using the terminology of Frey & Prinz (1978) and Kempton (1987). Representative clinopyroxene REE and multi-element patterns are shown in Fig. 3. LREE-depleted (type 1a) clinopyroxenes in peridotites have $La/Yb_{(N)}$ ratios <1 (0·05–0·69) and flat middle REE (MREE)–HREE patterns (e.g. KKJ0064, Fig. 3a). LREE-enriched (type 1b) clinopyroxenes in peridotites have $La/Yb_{(N)}$ >1 (1·4–9·3) (e.g. J10). Fractional melting of primitive mantle (spinel lherzolite) to the order of 5–10% can account for the MREE–HREE abundances in both type 1a and 1b clinopyroxenes. The pyroxenites exhibit significantly different patterns from the peridotites with convex-upward patterns that peak at Eu and give ratios of $La/Sm_{(N)} < 1$ and $Dy/Yb_{(N)} > 1$ (e.g. KKJ0037).

Multi-element patterns of the clinopyroxene separates are shown in Fig. 3b. Both type 1a and 1b clinopyroxenes display negative Nb, Zr and Ti anomalies. Type 1a clinopyroxenes are generally depleted in the most incompatible elements (i.e. Rb–Sm), except for positive U and variable Pb anomalies. Type 1b clinopyroxenes peak at Ce and generally have large negative Ba anomalies. The pyroxenites exhibit similar negative Nb, Zr and Ti anomalies to the peridotites but have steep concave-downward MREE–HREE patterns.

## Sr–Nd–Pb–Hf isotopes

Sr–Nd–Hf isotopic compositions of the clinopyroxene separates are shown in Fig. 4. Type 1a clinopyroxenes (white circles) have three of the highest Nd isotopic compositions in the dataset. Type 1b peridotites (grey circles) and the pyroxenites (black circles) exhibit a wide range of isotope ratios; that is, $^{143}Nd/^{144}Nd$ ~0·512710–0·513307 and $^{87}Sr/^{86}Sr$ ~0·70342–0·70245 (Fig. 4a). Some xenoliths are clearly more radiogenic than Red Sea MORB and the Afar plume (Volker *et al.*, 1993; Deniel *et al.*, 1994), and the range of compositions is similar to that of Saudi Arabian and Yemen mantle xenoliths (Henjes-Kunst *et al.*, 1990; Blusztajn *et al.*, 1995; Brueckner *et al.*, 1995; Baker *et al.*, 1998, 2002). Notably, no single Jordanian xenolith overlaps the field for Jordanian basalts, with the type 1b mantle clinopyroxenes characterized by lower $^{143}Nd/^{144}Nd$ for a given $^{87}Sr/^{86}Sr$ compared with the volcanic rocks.

Hf isotopes display a large range of compositions, from $^{176}Hf/^{177}Hf = 0·28279$ to 0·28751 (Fig. 4b and c), and extend to significantly more radiogenic values than is common in continental and oceanic volcanic rocks. As a comparison, the highest reported $^{176}Hf/^{177}Hf$ value for MORB is

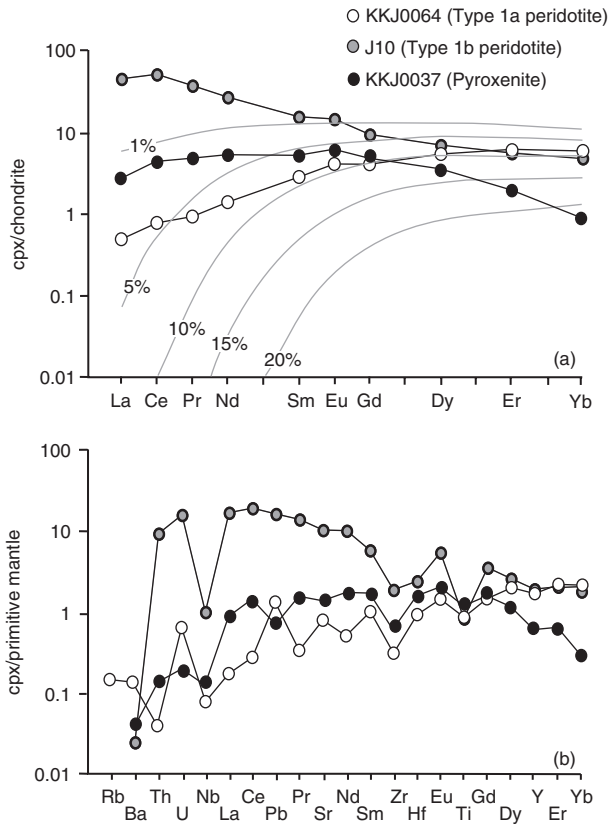


**Fig. 3.** (a) Representative chondrite-normalized REE patterns for type 1a and type 1b cpx in peridotites and cpx in pyroxenites. Normalization values are from McDonough & Sun (1995). Also shown are cpx compositions for residues of 1–20% partial melting of primitive mantle (McDonough & Sun, 1995) (spinel lherzolite: 0·55 ol, 0·25 opx, 0·18 cpx, 0·02 sp that melts in the proportions 0·1 ol, 0·2 opx, 0·68 cpx, 0·02 sp; Johnson *et al.*, 1990). Trace element abundances were calculated using the partition coefficients from the compilation by Ionov *et al.* (2002) and an algorithm from Johnson *et al.* (1990). (b) Primitive mantle (PM)-normalized multi-element patterns for representative samples. Normalization values are from McDonough & Sun (1995).

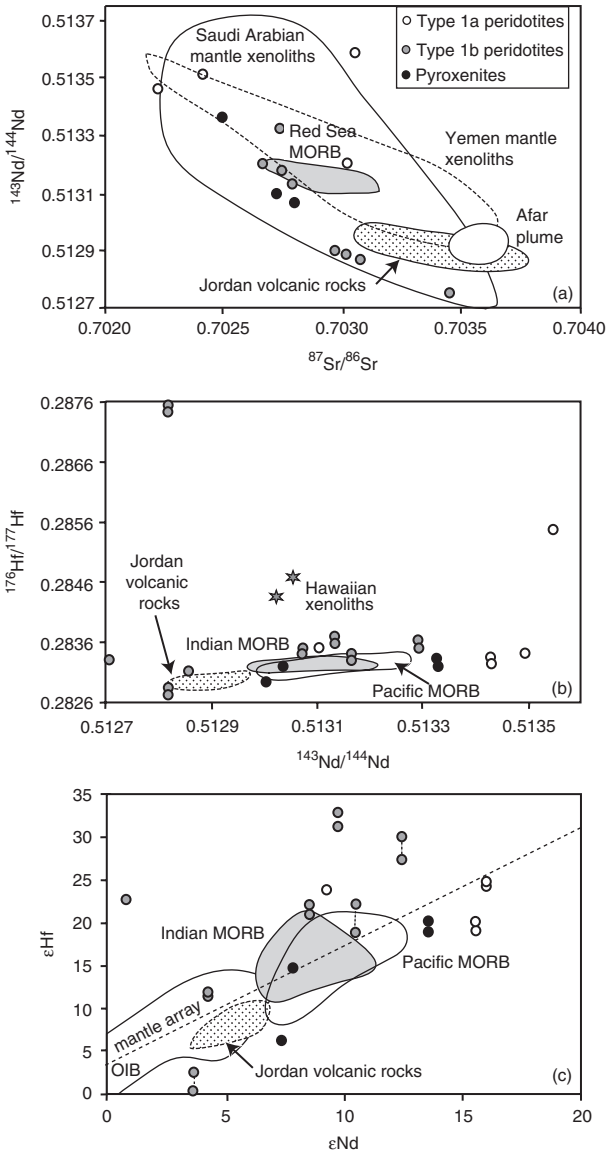


**Fig. 4.** (a) Nd–Sr isotopic compositions of clinopyroxene in Jordanian mantle xenoliths. Plotted for comparison are the isotopic compositions of Cenozoic Jordanian volcanic rocks, Saudi Arabian xenoliths (Henjes-Kunst *et al.*, 1990; Blusztajn *et al.*, 1995; Brueckner *et al.*, 1995), Yemen xenoliths (Baker *et al.*, 1998, 2002), Red Sea MORB (Volker *et al.*, 1993) and compositions representative of the Afar plume (Deniel *et al.*, 1994). (b) Nd–Hf isotopic compositions for Jordanian mantle xenoliths. Plotted for comparison are the fields for Pacific and Indian MORB (excluding three low $^{176}Hf/^{177}Hf$ and $^{143}Nd/^{144}Nd$ Indian MORB samples) (Chauvel & Blichert-Toft, 2001), two spinel lherzolites from Hawaii (Bizimis *et al.*, 2003) and the Jordanian volcanic rocks. (c) εNd–εHf for Jordanian mantle xenoliths (excluding the two highest $^{176}Hf/^{177}Hf$ samples). Also shown is the mantle array, the fields for Pacific and Indian MORB, and the field for OIB (Nowell *et al.*, 1998).

~0·2835 (Chauvel & Blichert-Toft, 2001). However, radiogenic $^{176}Hf/^{177}Hf$ ratios considerably higher than MORB values have been reported for a limited number of clinopyroxenes from mantle xenoliths from Hawaii (e.g. $^{176}Hf/^{177}Hf < 0·284630$; Bizimis *et al.*, 2003). It is also clear in Fig. 4b and c that Nd and Hf isotope ratios do not correlate well, in fact the highest $^{176}Hf/^{177}Hf$ sample has relatively low $^{143}Nd/^{144}Nd$ (0·512848) and the xenoliths do not overlap the Jordanian volcanic field in Hf–Nd isotopic space.

Pb isotope variations are illustrated in Fig. 5 and show a range of compositions from $^{206}Pb/^{204}Pb$ ~17·168 to 20·376. These Pb isotope ratios cover nearly the entire range observed in oceanic basalts, from MORB to HIMU basalts. The pyroxenites have $^{206}Pb/^{204}Pb$ values <19·007, and three out of four type 1a peridotites have low $^{206}Pb/^{204}Pb$ values (<18·594). A type 1a peridotite (KKJ0084) with high $^{206}Pb/^{204}Pb$ (~19·998) is relatively enriched in U and Th compared with the other type 1a xenoliths. This enrichment has clearly affected Pb isotopic

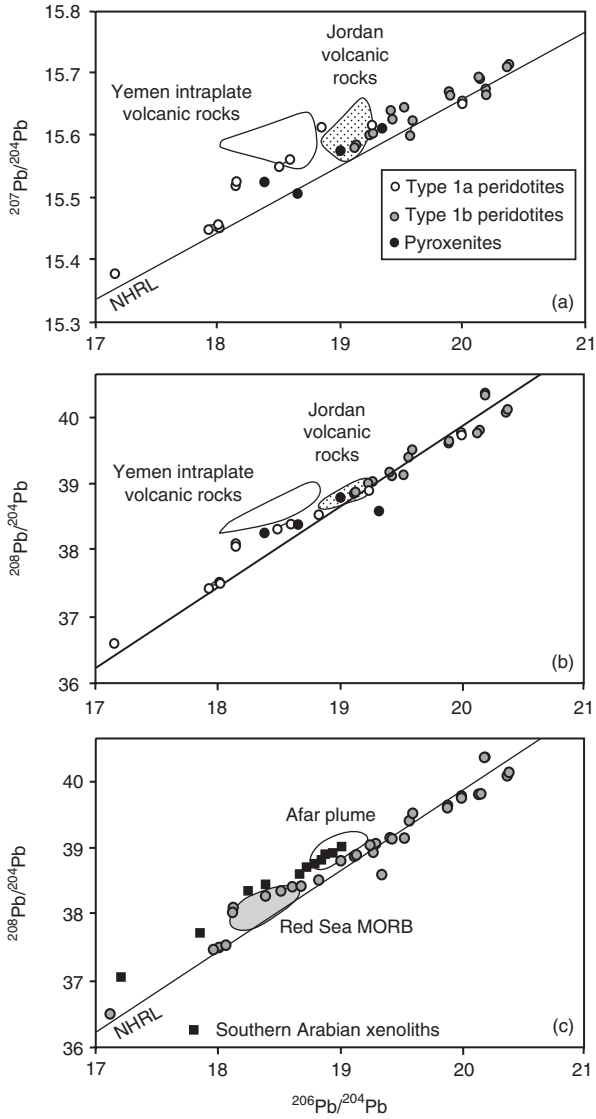


**Fig. 5.** (a) $^{207}Pb/^{204}Pb$–$^{206}Pb/^{204}Pb$ and (b) $^{208}Pb/^{204}Pb$–$^{206}Pb/^{204}Pb$ isotopic compositions for Jordanian mantle clinopyroxenes. Data for Jordanian and Yemen volcanic rocks are from (Shaw *et al.*, 2007). (c) A comparison of Jordanian (grey circles) and southern Arabian xenoliths (black squares) (Baker *et al.*, 1998, 2002), Red Sea MORB (Volker *et al.*, 1993) and Afar plume basalts (Deniel *et al.*, 1994). Northern Hemisphere Reference Line (NHRL) is from Hart (1984).

ratios while preserving a depleted $^{143}Nd/^{144}Nd$–$^{87}Sr/^{86}Sr$ type 1a signature with no significant LREE enrichment. Type 1b peridotites have relatively radiogenic Pb with $^{206}Pb/^{204}Pb$ ~19·129–20·376 with correspondingly unradiogenic $^{143}Nd/^{144}Nd$ and radiogenic $^{87}Sr/^{86}Sr$ values compared with type 1a peridotites. A small number of xenoliths overlap in Pb–Pb isotope space with the Jordanian volcanic rocks, but the Nd and Hf isotope ratios of these xenoliths are different from those of the basalts. Although the xenoliths display variations in $\triangle 7/4$Pb comparable with the Jordanian basalts (up to 7·9 in $\triangle 7/4$ vs 8·6 in $\triangle 7/4$ in the basalts), there is no systematic deviation from the Northern Hemisphere Reference Line (NHRL) as for the Jordanian basalts nor a distinct high $\triangle 7/4$ end-member component, which was interpreted to represent an enriched lithospheric mantle component in the volcanic source. If this hypothesis is correct, the xenoliths do not appear to represent the enriched lithospheric mantle source of the volcanic rocks.

Mantle xenoliths from Yemen have notably higher $^{208}Pb/^{204}Pb$ for a given $^{206}Pb/^{204}Pb$ than the Jordanian xenoliths and have values similar to Afar plume-derived Yemen volcanic rocks (Baker *et al.*, 1998, 2002) (Fig. 5b and c). There is also a lack of extremely radiogenic $^{206}Pb/^{204}Pb$ values in the Yemen xenoliths (e.g. southern Arabia $^{206}Pb/^{204}Pb \leq \sim 19$), implying that highly radiogenic Pb isotope mantle in northern Arabia is not sampled by the southern Arabian xenoliths or may have been overprinted by recent (Oligocene) pervasive Afar plume-related metasomatism (Baker *et al.*, 1998, 2002). The lack of an elevated $\triangle 8/4$ Afar plume signature in the Jordanian xenoliths is also consistent with the comparatively low $\triangle 8/4$ values of the Jordanian volcanic rocks (Shaw *et al.*, 2003) (Fig. 5b) and implies that the northern Arabian lithosphere was not influenced by Afar plume processes.

### Trace element–isotope correlations

Trace element ratios that are indicators of metasomatic processes, such as high La/Sm and La/Yb and low Ti/Eu and Zr/Hf, display correlations with Nd, Sr and Pb isotopes (e.g. Fig. 6a and b), suggesting that metasomatism is responsible for the enriched isotope and trace element signatures of type 1b xenoliths. In contrast, Hf isotopes do not correlate with trace element ratios or other isotopes. This observation, combined with the large range and extreme values of $^{176}Hf/^{177}Hf$ in the xenoliths compared with the Jordanian volcanic rocks and MORB, implies that Hf isotopes have been little affected by metasomatism and may preserve a pre-metasomatic mantle signature. The metasomatic media may be poor in Hf relative to the adjacent REE (Ionov & Weis, 2002) or Lu and Hf are more compatible during partial melting (higher cpx–melt partition coefficients) than Sm, Nd, Rb, Sr, U, Th and Pb and therefore tend to be less affected by metasomatism (Vervoort & Blichert-Toft, 1999).

## DISCUSSION

Briefly to summarize the findings thus far, the Jordanian xenoliths appear to have undergone variable degrees of metasomatic enrichment, which is reflected in their highly variable LREE/HREE and large ion lithophile element to high field strength element (LILE/HFSE) ratios.

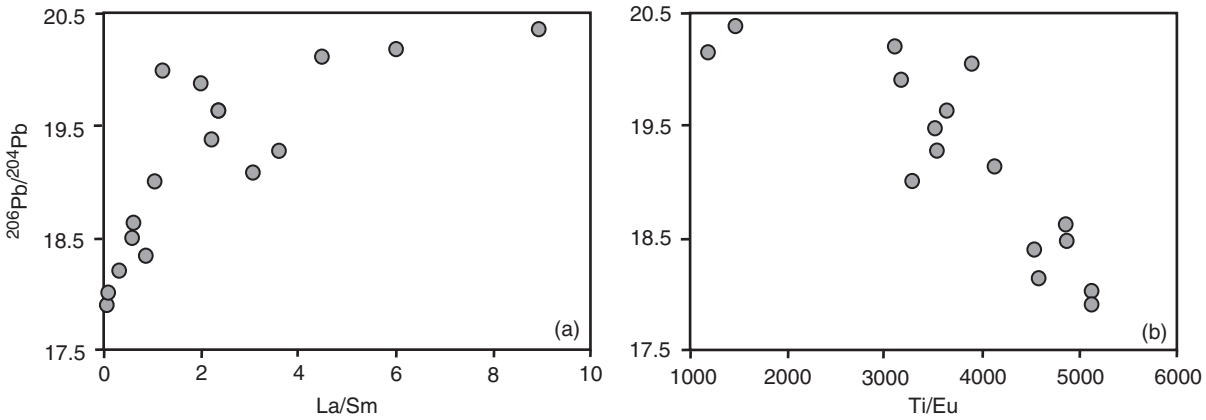


**Fig. 6.** (a) $^{206}Pb/^{204}Pb$ vs La/Sm and (b) $^{206}Pb/^{204}Pb$ vs Ti/Eu, illustrating the correlations between trace element ratios (as indicators of metasomatism) and Pb isotopes.

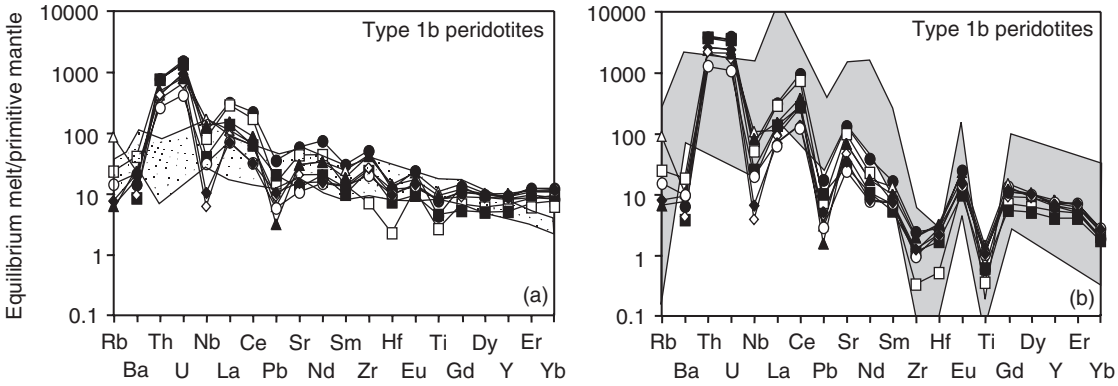


**Fig. 7.** (a) PM-normalized trace element patterns for calculated melt compositions in equilibrium with clinopyroxene using high-pressure $D_{cpx/mafic\ silicate\ melt}$. Partition coefficients are from Blundy & Dalton (2000) (Rb, Ba, Nb, La, Pb, Sr, Nd, Sm and Zr), Hauri *et al.* (1994) (Th and U), Hart & Dunn (1993) (Ce), Johnson (1998) (Hf) and Green *et al.* (2000) (Eu, Gd, Dy, Er, Yb and Y). Plotted for comparison is the field for the Jordanian basalts. (b) PM-normalized trace element patterns for calculated melt compositions in equilibrium with clinopyroxene using $D_{cpx/carbonatitic\ melt}$. Partition coefficients are from Blundy & Dalton (2000) (Rb, Ba, Nb, La, Pb, Sr, Nd, Sm, Zr, Yb and Ti), Adam & Green (2001) (Ce and Hf), Klemme *et al.* (1995) (Eu, Ti, Gd, Dy, Y and Er) and Hauri *et al.* (1993) (Th and U). Plotted for comparison is the field for East African rift carbonatites (Bizimis *et al.*, 2003).

Isotopically, the xenoliths encompass a wide range of compositions that reflect this metasomatism and/or the response to radiogenic ingrowth as a result of variable parent–daughter ratios (e.g. U/Pb). In terms of Pb isotopes, the xenoliths cover nearly the entire range of values displayed by oceanic basalts and individual samples are isotopically heterogeneous. Hf and Nd isotopes do not correlate and the most radiogenic $^{176}Hf/^{177}Hf$ ratios from this study significantly exceed the highest reported $^{176}Hf/^{177}Hf$ ratios for MORB. Moreover, isotopically, no individual xenolith appears to represent an appropriate source for Jordanian intraplate volcanism. In the following section, the sources and mechanisms of metasomatism are assessed, a model is developed for the evolution of the Arabian lithospheric mantle, and the possibility that these xenoliths represent a mantle source for the Cenozoic volcanism is evaluated.

## Constraining metasomatic processes

### *Assessing possible metasomatic agents using equilibrium melt models*

Melt compositions in equilibrium with clinopyroxene have been calculated for the metasomatized type 1b peridotites to assess the nature of the metasomatic agents involved in mantle enrichment processes. Two types of clinopyroxene–melt partition coefficients have been utilized, $D_{cpx/mafic\ silicate\ melt}$ and $D_{cpx/carbonatite}$, and the results are shown in Fig. 7. Calculated mafic silicate melts in equilibrium with type 1b clinopyroxenes have different primitive mantle (PM)-normalized trace element patterns to the Jordanian basalts. In particular, the calculated melts are highly enriched in Th and U and depleted in Nb, whereas the Jordanian basalts have large positive Nb and negative Th anomalies (Fig. 7a). Thus, a mafic silicate melt similar to the Jordanian volcanic rocks is unlikely to

be the metasomatic agent responsible for type 1b clinopyroxenes. In contrast, carbonatitic melts in equilibrium with the peridotites display remarkably similar concentrations and patterns to East African carbonatites, with their prominent positive U and Th anomalies and negative Nb, Pb, Zr, Ti and Hf anomalies (Fig. 7b). If the metasomatic agent was a silicate melt, there would have been concomitant enrichment of the HFSE as well as the LILE and LREE (Downes, 2001).

One feature of the calculated Jordanian melt compositions that is unusual for carbonatites is the large depletions in Nb and high La/Nb ratios (0·6–22·8) (versus carbonatite La/Nb ~0·51; Woolley & Kempe, 1989). Nb also does not correlate with indices of metasomatism, such as LILE–LREE enrichment and Nd–Sr–Pb isotopes, and appears to be decoupled from the other HFSE. Nb depletion may therefore be a source feature of the Arabian mantle.

The composition of the metasomatic agent places constraints on the depth at which these processes occurred. Carbonate is stable at high pressures (>16 kbar), therefore any free fluid above that required to fully hydrate mica will be $H_2O$-rich at high pressures (Eggler, 1987). At low pressures where carbonate breaks down and $H_2O$ tends to partition into silicate melts, a $CO_2$-rich fluid is available to metasomatize portions of the mantle. Shallow-level carbonatitic or $CO_2$-rich metasomatism is also consistent with pressure–temperature estimates that imply shallow equilibration depths. This is a feasible situation in a subduction-zone setting, where the hydrous component from the original slab-derived fluid is exhausted by reactions in the deep mantle and therefore the residual fluid is largely $CO_2$-rich at shallow levels (Ionov *et al.*, 1995). Recent studies on the East African rift xenoliths (Bedini *et al.*, 1997) have shown both carbonatitic and silicic metasomatism occurring on a kilometre scale, involving gradual solidification of melt infiltrated into the lithospheric mantle through successive melt–rock reactions down a conductive, thermal gradient. This process is associated with a strong chemical evolution of the melt, from an original basaltic composition to progressively volatile-enriched compositions, culminating in low-$T$, small-volume carbonatitic melts. Stein *et al.* (1997) developed a model for chromatographic metasomatism of the Arabian lithosphere, based on a subduction-zone environment that is known to have been active in Arabia ~600–900 Myr ago. In particular, Nb is concentrated near of the base of the supra-subduction zone mantle wedge, because of its relative compatibility and highly immobile character, and its concentration front migrates slowly compared with the fronts of highly incompatible elements, which migrate rapidly. Nb does not reach the upper zone of the column and therefore its concentration in the middle of the wedge is the same as the original wedge concentration. These Nb-poor and Nb-rich zones in the mantle wedge later fossilize and become part of the lithospheric mantle. In the context of our data for Jordanian volcanic rocks and xenoliths, the Nb-depleted mantle xenoliths may have sampled the upper, Nb-depleted portion of the fossilized mantle wedge above the Nb concentration front, whereas the Nb-enriched Jordanian basalts were generated in Nb-rich mantle near the base of the fossilized mantle wedge.

### *The timing of metasomatism*

There is no isotopic evidence to support recent (<30 Ma) metasomatism of the northern Arabian mantle by the Afar plume, unlike the xenoliths hosted in alkali basalts from Yemen. Jordanian xenolith Sr and Nd isotopic signatures do not overlap with Afar plume compositions and the plume does not constitute a Pb isotope end-member as it does for the Yemen xenoliths. These findings are consistent with previous work on the Jordanian volcanic rocks (Shaw *et al.*, 2003), which did not show any evidence that the Afar plume was channelled northwards beneath northern Arabia.

Previous workers have suggested that a widespread metasomatic event of Pan-African age (~600–700 Ma) affected the Arabian lithospheric mantle (Brueckner *et al.*, 1995; Henjes-Kunst *et al.*, 1990; Blusztajn *et al.*, 1995; Baker *et al.*, 2002) and was related to island-arc volcanism at this time (Stoeser & Camp, 1985). The concurrence of metasomatism and island-arc activity provides a plausible source for the metasomatic agent in the form of slab-derived fluids or small-degree partial melts in response to hydration of the mantle wedge by dehydration of the subducting slab. A 600 Ma depleted mantle 'reference isochron' is illustrated on a $^{147}Sm/^{144}Sm$–$^{143}Nd/^{144}Nd$ diagram in Fig. 8a, along with the field for Saudi Arabian and Yemen xenoliths (Brueckner *et al.*, 1995; Henjes-Kunst *et al.*, 1990; Blusztajn *et al.*, 1995; Baker *et al.*, 2002). There is some scatter within the Jordanian dataset and the isotopically most enriched xenoliths (J10 and J11) lie above the 600 Ma 'isochron', suggesting that these xenoliths had an initial εNd higher than depleted mantle at the time of their formation or that the metasomatism is younger than 600 Ma. The former situation is unlikely if the metasomatic melts were derived from a plume or subduction zone (e.g. recycled oceanic crust would have a depleted mantle MORB signature) but the mantle may have already been extremely heterogeneous at 600 Ma, with εNd compositions both higher and lower than depleted mantle, and metasomatism may not have completely overprinted this at the time of subduction. Although such extreme Nd isotope heterogeneity is not observed today ($\varepsilon Nd_{present\ day} = 1{\cdot}4$–$17{\cdot}5$), the large range of unmetasomatized εHf values illustrates the extent of isotopic heterogeneity that existed in the proto-Arabian lithospheric mantle prior to metasomatism (e.g. $\varepsilon Hf_{(700\ Ma)}$ ~4·8–100·6 vs $\varepsilon Hf_{(700\ Ma\ DM)}$ ~12·7).

If metasomatism was younger than 600 Ma, it may be related to Mesozoic rifting and magmatism occurring

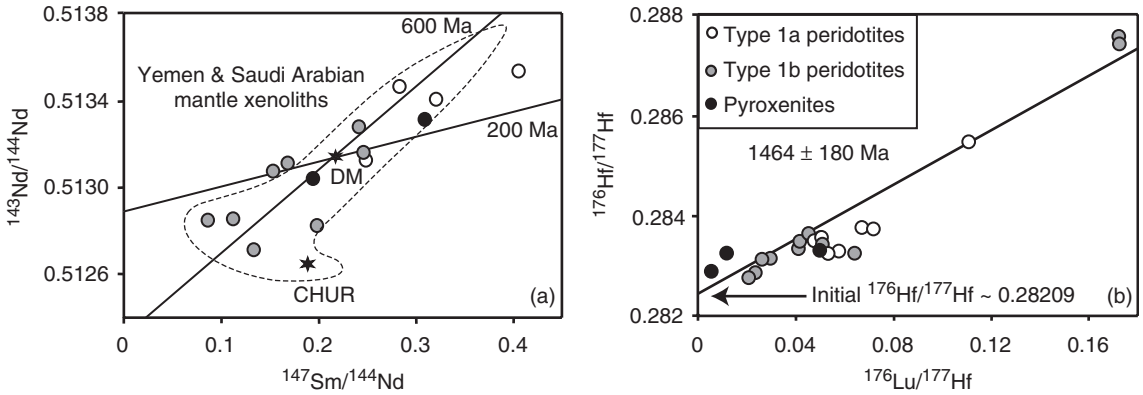


**Fig. 8.** (a) $^{147}Sm/^{144}Nd$ vs $^{143}Nd/^{144}Nd$ in Jordanian, Saudi Arabian and Yemen mantle xenoliths. Also plotted are 600 Ma and 200 Ma reference isochrons for depleted mantle. $^{147}Sm/^{144}Nd$ ratios for the Jordanian xenoliths were calculated from elemental Sm and Nd trace element data. (b) $^{176}Lu/^{177}Hf$ vs $^{176}Hf/^{177}Hf$ showing the clinopyroxene 1464 ± 180 Ma 'errorchron'.

along the western edge of the Arabian Peninsula from Egypt to Syria (Ben-Gai & Ben-Avraham, 1995). Rifting could have remobilized components within the lithosphere that were related to earlier Pan-African subduction-zone activity or allowed small-degree asthenospheric melts to infiltrate and variably metasomatize parts of the lithospheric mantle. Cretaceous basalts (115 Ma) from Israel have comparable Pb isotopic signatures to the most enriched Jordanian xenoliths (Stein & Hofmann, 1992) and the isotopic heterogeneity of the Phanerozoic Israeli alkali basalts has been attributed as the product of a 'fossilized' plume head that was unable to penetrate the continental lithosphere and was therefore trapped and stored beneath it (Stein & Hofmann, 1992). The plume head was inferred to have been emplaced some time between late Proterozoic crust formation and the initiation of Phanerozoic magmatic cycles 200 Myr ago. The plume signature was diluted by overlying mantle material and periodically tapped as the lithosphere rifted and thinned. A 200 Ma 'reference isochron' is depicted in Fig. 8a and lies above the most enriched samples, thus providing a minimum age for the metasomatic event. Depleted mantle Nd model ages for the Jordanian clinopyroxenes range from 270 to 909 Ma and provide little evidence to further constrain a metasomatic event. Back-calculated 200 Ma Pb isotopic signatures for the most enriched Jordanian xenoliths, using average measured U/Pb ratios, give Pb isotope signatures significantly more radiogenic than 200 Ma MORB. The metasomatic event must be at least 600 Ma or older for age-corrected Pb isotope ratios for the Jordanian clinopyroxenes to fall within the range of coexisting MORB at that time, thus tentatively linking metasomatism with Pan-African-related tectonic processes rather than younger rifting events.

## The age of the Arabian lithospheric mantle

The Arabian–Nubian shield is composed of a series of juvenile island-arc terranes and micro-continental fragments accreted during the late Precambrian (Pan-African ~950–630 Ma) (Stoeser & Camp, 1985; Windley *et al.*, 1996). The isotopically depleted nature of Pan-African crust has been well documented in recent years (e.g. Duyverman *et al.*, 1982; Claesson *et al.*, 1984; Stern & Kröner, 1993; Stein & Goldstein, 1996; Stern & Abdelsalam, 1998; Vervoort & Blichert-Toft, 1999), with Nd and Hf isotope ratios ranging from $\varepsilon Nd_{(t)} \sim +6{\cdot}6$ to $+7{\cdot}7$ and $\varepsilon Hf_{(t)} \sim +10{\cdot}9$ to $+15{\cdot}5$. There is also evidence for the existence of older early Proterozoic–late Archean terranes in southern Arabia (Yemen), which have been dated at 1·7–2·9 Ma (Windley *et al.*, 1996; Whitehouse *et al.*, 1998) and an Archean crustal component is thought to have played a role in the genesis of Oligocene flood volcanism and intraplate volcanism in Yemen (Baker *et al.*, 1996, 1997). In contrast to Yemen, there is no evidence for the presence of Archean crust in northern Arabia or the involvement of an Archean crustal component during the petrogenesis of Jordanian volcanic rocks (Shaw *et al.*, 2003).

The coupled nature of crust and lithospheric mantle imply that the Arabian mantle from which the xenoliths were derived is broadly the same age as the overlying crust, as the depleted nature of type la peridotites is consistent with Pan-African crustal signatures. However, the apparent resistance of Hf isotopes to metasomatism potentially provides important constraints on the evolution of the proto-Arabian lithospheric mantle. Lu–Hf clinopyroxene data define a poorly constrained errorchron of ~1464 ± 180 Ma, with an initial $^{176}Hf/^{177}Hf$ ratio of 0·28209 ($\varepsilon Hf_{(t)} \sim 6{\cdot}6$) (Fig. 8b) whereas Lu–Hf Chondritic Uniform Reservoir (CHUR) model ages for the majority of xenoliths from both Jordan and Yemen are between 1205 and 1856 Ma. These ages may correspond to a period of major mantle depletion that pre-dates the formation of the Pan-African lithosphere. Simple calculations based on the highest measured $^{176}Lu/^{177}Hf$ ratio of the sample set suggest that the range of observed $^{176}Hf/^{177}Hf$

ratios (167 εHf units) can be produced from a CHUR-like mantle reservoir in ~1750 Myr. The above timeframe is comparable with previous estimates of depletion events (1·3–1·9 Ga) (Henjes-Kunst *et al.*, 1990; Blusztajn *et al.*, 1995) in the Arabian lithosphere, calculated from Nd model ages. Although the evolution of Hf isotopes is unlikely to have been a simple one-stage process and multiple depletion events have probably occurred, the fractionation of Lu and Hf and the generation of sufficiently high Lu/Hf ratios (~1·2) can be produced by ~10% fractional melting of a primitive spinel lherzolite mantle source, consistent with partial melting estimates from PM-normalized REE patterns (Fig. 2a). A melting event of this extent would also significantly fractionate Sm and Nd, resulting in an increase of ~116 εNd units from primitive mantle in 1750 Myr, but subsequently erased $^{143}Nd/^{144}Nd$ heterogeneities through metasomatism. The comparatively small present-day variation in εNd (1–18 units) supports this theory.

## Implications for the source of Jordanian volcanism

Previous studies of Jordanian volcanism (Shaw *et al.*, 2003) suggested that the parental rocks were probably derived from a mixed asthenospheric–lithospheric source. At first glance, the isotopic dissimilarity between the Jordanian basalts and the mantle xenoliths implies that they cannot have had the same lithospheric mantle source. The lithospheric mantle isotope signature of Jordanian volcanic rocks is also not simply the result of melt averaging. For example, the weighted average isotopic compositions of all the xenoliths for $^{176}Hf/^{177}Hf$ and $^{206}Pb/^{204}Pb$ are ~0·283475 and 19·829, respectively, too high to be a suitable end-member for the volcanic rocks ($^{176}Hf/^{177}Hf$ ~0·2829 and $^{206}Pb/^{204}Pb$ ~19·2). Simple mixtures of a type 1a peridotite and type 1b peridotite also cannot reproduce the volcanic rock compositions. A pyroxenite source for the Jordanian basalts can probably be ruled out on the basis of the weighted isotopic averages for $^{143}Nd/^{144}Nd$, $^{176}Hf/^{177}Hf$ and $^{206}Pb/^{204}Pb$ (0·513138, 0·283265 and 18·863, respectively). These values are too high (averages $^{143}Nd/^{144}Nd$ ~0·5129 and $^{176}Hf/^{177}Hf$ ~0·2829) and too low ($^{206}Pb/^{204}Pb$ ~19·0) respectively to represent an appropriate source for the Jordanian volcanic rocks.

An explanation for the dissimilarity between the volcanic rocks and the lithosphere-derived xenoliths is that the volcanic rocks were generated solely within the asthenosphere. This is not plausible because the chemically and isotopically distinct volcanic end-members require isolation from one another, which is unlikely if both were generated in the convecting asthenospheric mantle. Also, on the basis of REE modelling, the magma generation process occurred over an extended depth range in the mantle with a change from early shallow spinel-facies melts to deeper garnet-facies melts as rifting progressed. The thickness of the Arabian lithosphere prior to Miocene rifting (~100–120 km) (Mooney *et al.*, 1985) suggests that initial spinel-facies melts (e.g. <80 km) that were generated before significant lithospheric thinning took place could not be derived from the asthenosphere (e.g. >100–120 km).

An alternative scenario is that the lithosphere is isotopically zoned and that the basaltic magmas were generated within a different part of the lithosphere from the xenoliths. This model is plausible considering that the xenoliths were derived from shallow lithospheric mantle levels just below the crust–mantle boundary. There is no petrographic or chemical evidence to suggest that the xenoliths were generated from deeper levels in the asthenosphere but re-equilibrated at shallow lithospheric levels in response to Miocene rifting. If this were the case, we might expect to see remnants of garnet in the mineral assemblage or clinopyroxene showing trace element characteristics of garnet. In addition, the large range of isotopic heterogeneity displayed by the xenoliths is unlikely to be a feature of the convecting asthenosphere. The depth of the basaltic magma lithospheric source is more difficult to ascertain but its Nb-enriched character and high $\Delta 7/4$ signature, which is thought to represent a subducted sediment component in the mantle (Shaw *et al.*, 2007), suggest a lower lithospheric source close to the base of the fossilized mantle wedge. This model disagrees with that of Stein & Hofmann (1992), who proposed an asthenospheric mantle source and 'fossilized' plume head for the Mesozoic Israeli basalt, to account for large variations in Pb isotope signatures ($^{206}Pb/^{204}Pb$ ~19·09–20·41) and their isotopic dissimilarity to the Israeli mantle xenoliths. We suggest, however, that there is no need to invoke a plume beneath northern Arabia for the following reasons. (1) The lack of isotopic similarity between the Israeli xenoliths and the volcanic rocks does not exclude the volcanic rocks from having a lithospheric source if the lithosphere is isotopically zoned. (2) The most enriched Israeli basalts ($^{206}Pb/^{204}Pb_{(0)}$ ~20·41) are identical to the enriched Jordanian xenoliths and could, therefore, be generated from Pan-African metasomatized lithospheric mantle. Interestingly, the 80–200 Ma Israeli basalts have a much larger range of Pb isotope compositions compared with the <20 Ma basalts, which are isotopically similar to <15 Ma Jordanian basalts. Mesozoic basalts may therefore have been derived from a shallow mantle source that is compositionally similar to the Jordanian xenoliths, whereas the younger volcanism in Israel and Jordan perhaps tapped a deeper mantle source in response to late Miocene thinning and rifting of the lithosphere.

## The evolution of the Arabian mantle

The debate over the generation and stabilization of continental lithosphere is a fundamental problem in Earth Sciences (Stein & Goldstein, 1996). It has been

conventionally viewed as occurring through arc magmatism at convergent plate margins. However, Stein & Goldstein (1996) suggested that hotspot volcanism and underplating were important processes in creating the Arabian shield, based on the fact that early lavas (>950 Ma) were too thick (>16 km) to represent normal oceanic crust, even taking into account subsequent tectonic thickening. The high crust formation rate suggested that processes other than arc magmatism had played a role in crust generation. However, Stein & Goldstein did not preclude arc-accretion during development of Arabian lithosphere and suggested that oceanic lithosphere was modified by subduction at the margins, accounting for the formation of large continental segments that occurred during short episodes between 950 and 650 Ma and their calc-alkaline affinities (Bentor, 1985; Stein & Goldstein, 1996). One line of evidence that is difficult to reconcile with plume-related volcanism is the isotopically depleted nature of some of the Jordanian mantle xenoliths, which are similar to, or more depleted than MORB. This is in contrast to Stein & Goldstein's (1996) model, which suggested that Arabian mantle xenoliths are relatively isotopically enriched compared with MORB and are probably derived from plume-type enriched lithospheric mantle. If a plume dominated the mantle prior to arc magmatism it clearly did not contaminate or infiltrate all areas of the Jordanian lithospheric mantle.

Taking into account previous models and the results of this study, we suggest that the evolution of the Arabian lithosphere beneath Jordan is as follows. The proto-Arabian lithospheric mantle underwent a major melting event in early Proterozoic–late Archean times (at the earliest at ~1·2 Ga). This event was followed by island-arc volcanism and major crust formation during the Pan-African orogeny, which occurred ~950–600 Myr ago (Stoeser & Camp, 1985). During subduction, the dehydration of oceanic crust and sediment liberated fluids and possibly small-degree melts into the mantle, creating zones of enrichment for certain elements depending upon their compatibility. For example, the compatibility and immobility of Nb relative to LILE and LREE meant that it was concentrated near the base of the mantle wedge whereas the upper part of the wedge retained its original depleted Nb signature. Small amounts of pelagic sediment from the slab may have also been incorporated into the mantle at the base of the wedge. Other mobile elements in the fluid or melt (LREE and LILE) were transported up through the mantle wedge. At deep lithospheric levels (>16 kbar) the fluid was probably $H_2O$-rich, whereas at shallow lithospheric levels (i.e. the source of the Jordanian xenoliths) the fluid was $CO_2$-rich (LILE-enriched and HFSE-depleted, particularly in Hf), because of the instability of carbonate at <16 kbar (equivalent to 50 km) (Eggler, 1987). Following subduction, the mantle wedge fossilized, preserving enriched and depleted zones. Lithospheric thinning and rifting began in the Miocene (~15 Ma) triggering partial melting of spinel-facies mantle in the lower lithosphere. Further rifting and thinning allowed these spinel-facies melts to mix with melts derived from deeper, asthenospheric garnet-facies mantle. *En route* to the surface, the melts entrained segments of variably carbonatitic-metasomatized shallow lithospheric mantle.

## CONCLUSIONS

The following conclusions can be drawn from this study.

(1) The Arabian lithospheric mantle beneath Jordan is chemically and isotopically heterogeneous. Clinopyroxenes from the peridotites are variably Th–U–LILE–LREE enriched and display prominent negative Nb, Zr, Hf and Ti anomalies. The Nd–Sr–Pb–Hf isotopic data for both the peridotites and the pyroxenites encompass values more radiogenic than MORB. Pb isotopes display a range of values comparable with the entire oceanic basalt array. Some εHf values are some of the highest ever recorded in mantle samples and are decoupled from εNd in the same samples.

(2) Isotopic and elemental correlations suggest that the xenoliths have been metasomatized by a carbonatitic melt or fluid, probably during Pan-African subduction. There is no evidence for recent metasomatism (<30 Ma) related to the Afar plume like that postulated to have affected the southern Arabian lithospheric mantle. Subduction processes liberated fluids and possibly small-degree melts from the dehydrating slab, which travelled up through the mantle wedge and variably enriched parts of the mantle. After subduction ceased, the mantle wedge fossilized and preserved chemically and isotopically distinct zones until the onset of Miocene rifting. This initiated partial melting of the spinel-facies mantle in the lower lithosphere and later asthenospheric garnet-facies melts, which entrained metasomatized shallow lithospheric mantle *en route* to the surface.

(3) Hf isotopes were not affected by Pan-African metasomatic events and therefore record signatures of ancient (>1·2 Ga) pre-metasomatic upper mantle, which was the protolith of the present Arabian lithospheric mantle. The 'resistance' of the Lu–Hf isotopic system to metasomatism has resulted in the development of extremely heterogeneous Hf isotopic signatures over time that are decoupled from other isotopic systems.

(4) No individual mantle sample exactly matches the chemical and isotopic signature of Jordanian intraplate volcanism. It is possible that the volcanic rocks were sourced from the lower lithosphere close to the base of the fossilized mantle wedge whereas the xenoliths were generated at shallow lithospheric depths close to the crust–mantle boundary. Melt 'averaging' may obscure

some of the isotopic heterogeneity observed in the xenoliths when the upper mantle is sampled by volcanism.

(5) These conclusions are consistent with previous models for the development of Arabian lithospheric mantle, although the new high-precision Pb and Hf isotope data have provided new insights into the long and complex history of sub-continental mantle and its relationship to recent volcanic activity. Further Hf and Pb isotope studies of mantle xenoliths from sub-continental, sub-oceanic and sub-arc settings may shed some light on the complex histories of lithospheric mantle worldwide. The robustness of the Lu–Hf isotopic system to alteration by metasomatic processes suggests that it is a valuable tool for identifying crust–mantle differentiation throughout Earth's history and the age of mantle source regions.

## ACKNOWLEDGEMENTS

We thank Kristine Krogh Jensen and Chris Hieronymus for assistance with data analysis. The Danish Lithosphere Centre and Royal Holloway University of London are thanked for the joint funding of a Ph.D. studentship that made this project possible. Hannes Brueckner and Ian Parkinson are thanked for their comments on an earlier version of this manuscript.

## REFERENCES

Adam, J. & Green, T. (2001). Experimentally determined partition coefficients for minor and trace elements in peridotite minerals and carbonatitic melt, and their relevance to natural carbonatites. *European Journal of Mineralogy* **13**, 815–827.

Baker, J. A., Thirlwall, M. F. & Menzies, M. A. (1996). Sr–Nd–Pb and trace element evidence for crustal contamination of plume-derived flood basalts: Oligocene flood volcanism in western Yemen. *Geochimica et Cosmochimica Acta* **60**, 2559–2581.

Baker, J. A., Menzies, M. A., Thirlwall, M. F. & Macpherson, C. G. (1997). Petrogenesis of Quaternary intraplate volcanism, Sana'a, Yemen: implications for plume–lithosphere interaction and polybaric melt hybridization. *Journal of Petrology* **38**, 1359–1390.

Baker, J., Chazot, G., Menzies, M. & Thirlwall, M. (1998). Metasomatism of the shallow mantle beneath Yemen by the Afar plume—implications for mantle plumes, flood volcanism, and intraplate volcanism. *Geology* **26**, 431–434.

Baker, J., Chazot, G., Menzies, M. A. & Thirlwall, M. (2002). Lithospheric mantle beneath Arabia: A Pan-African protolith modified by the Afar and older plumes, rather than a source for continental volcanism? In: Menzies, M. A., Klemperer, S. L., Ebinger, C. J. & Baker, J. (eds) *Volcanic Rifted Margins. Geological Society of America, Special Papers* **362**, 65–80.

Baker, J., Waight, T. & Meyzen, C. (2004). Pb isotopic analysis of standards and samples using a $^{207}Pb$–$^{204}Pb$ double spike and thallium to correct for mass bias with a double focusing MC-ICP-MS. *Chemical Geology* **211**, 275–303.

Bedini, R. M., Bodinier, J.-L., Dautria, J.-M. & Morten, L. (1997). Evolution of LILE-enriched small melt fractions in the lithospheric mantle: a case study from the East African Rift. *Earth and Planetary Science Letters* **153**, 67–83.

Ben-Gai, Y. & Ben-Avraham, Z. (1995). Tectonic processes in offshore northern Israel and the evolution of the Carmel structure. *Marine and Petroleum Geology* **12**, 553–568.

Bentor, Y. K. (1985). The crustal evolution of the Arabo-Nubian massif with special reference to the Sinai peninsula. *Precambrian Research* **28**, 1–74.

Bizimis, M., Salters, V. J. M. & Dawson, J. B. (2003). The brevity of carbonatite sources in the mantle: evidence from Hf isotopes. *Contributions to Mineralogy and Petrology* **145**, 281–300.

Bizzarro, M., Baker, J. A. & Ulfbeck, D. (2003). New digestion and chemical techniques for rapid and highly reproducible determination of Lu/Hf and Hf isotope ratios in geological materials by MC-ICP-MS. *Geostandards Newsletter* **27**, 133–145.

Blundy, J. D. & Dalton, J. A. (2000). Experimental comparison of trace element partitioning between clinopyroxene and melt in carbonate and silicate systems, and implications for mantle metasomatism. *Contributions to Mineralogy and Petrology* **139**, 356–371.

Blusztajn, J., Hart, S. R., Shimizu, N. & McGuire, A. V. (1995). Trace-element and isotopic characteristics of spinel peridotite xenoliths from Saudi Arabia. *Chemical Geology* **123**, 53–65.

Bodinier, J. L., Vasseur, G., Vernières, J., Dupuy, C. & Fabriès, J. (1990). Mechanisms of mantle metasomatism: geochemical evidence from the Lherz orogenic peridotite. *Journal of Petrology* **31**, 597–628.

Bodinier, J. L., Menzies, M. A., Shimizu, N., Frey, F. A. & McPherson, E. (2004). Silicate, hydrous and carbonate metasomatism at Lherz, France: Contemporaneous derivatives of silicate melt–harzburgite reaction. *Journal of Petrology* **45**, 299–320.

Brueckner, H. K., Elhaddad, M. A., Hamelin, B., Hemming, S., Kröner, A., Reisberg, L. & Seyler, M. (1995). A Pan-African origin and uplift for the gneisses and peridotites of Zabargad Island, Red Sea: A Nd, Sr, Pb, and Os isotope study. *Journal of Geophysical Research* **100**, 22283–22297.

Chauvel, C. & Blichert-Toft, J. (2001). A hafnium isotope and trace element perspective on melting of the depleted mantle. *Earth and Planetary Science Letters* **190**, 137–151.

Claesson, S., Pallister, J. S. & Tatsumoto, M. (1984). Samarium–neodymium data on two late Proterozoic ophiolites of Saudi Arabia and implications for crustal and mantle evolution. *Contributions to Mineralogy and Petrology* **85**, 244–252.

Deniel, C., Vidal, P., Coulon, C., Vellutini, P.-J. & Piquet, P. (1994). Temporal evolution of mantle sources during continental rifting: The volcanism of Djibouti (Afar). *Journal of Geophysical Research* **99**, 2853–2869.

Downes, H. (2001). Formation and modification of the shallow subcontinental lithospheric mantle: a review of geochemical evidence from ultramafic xenolith suites and tectonically emplaced massifs of western and central Europe. *Journal of Petrology* **42**, 233–250.

Duyverman, H. J., Harris, N. B. W. & Hawkesworth, C. J. (1982). Crustal accretion in the Pan-African: Nd and Sr isotope evidence from the Arabian Shield. *Earth and Planetary Science Letters* **59**, 315–326.

Eggler, D. H. (1987). Solubility of major and trace elements in mantle metasomatic fluids: experimental constraints. In: Menzies, M. A. & Hawkesworth, C. J. (eds) *Mantle Metasomatism*. London: Academic Press, pp. 21–39.

El-Isa, Z., Mechie, J., Prodehl, C., Makris, J. & Rihm, R. (1987). A crustal structure study of Jordan derived from seismic refraction data. *Tectonophysics* **138**, 235–253.

Frey, F. A. & Prinz, M. (1978). Ultramafic inclusions from San Carlos, Arizona: Petrologic and geochemical data bearing on their petrogenesis. *Earth and Planetary Science Letters* **38**, 129–176.

Green, T. H., Blundy, J. D., Adam, J. & Yaxley, G. M. (2000). SIMS determination of trace element partition coefficients between garnet, clinopyroxene and hydrous basaltic liquids at 2–7·5 GPa and 1080–1200°C. *Lithos* **53**, 165–187.

Hart, S. R. (1984). A large-scale isotope anomaly in the Southern Hemisphere mantle. *Nature* **309**, 753–757.

Hart, S. R. & Dunn, T. (1993). Experimental cpx/melt partitioning of 24 trace elements. *Contributions to Mineralogy and Petrology* **113**, 1–8.

Hauri, E. H., Shimizu, N., Dieu, J. J. & Hart, S. R. (1993). Evidence for hot-spot related carbonatite metasomatism in the oceanic upper mantle. *Nature* **365**, 221–227.

Hauri, E. H., Wagner, T. P. & Grove, T. L. (1994). Experimental and natural partitioning of Th, U, Pb and other trace elements between garnet, clinopyroxene and basaltic melts. *Chemical Geology* **117**, 149–166.

Henjes-Kunst, F., Altherr, R. & Baumann, A. (1990). Evolution and composition of the lithospheric mantle underneath the western Arabian peninsula: constraints from Sr–Nd isotope systematics of mantle xenoliths. *Contributions to Mineralogy and Petrology* **105**, 460–472.

Ionov, D. A. & Weis, D. (2002). Hf isotope composition of mantle peridotites: first results and inferences for the age and evolution of the lithospheric mantle. *International Conference on Orogenic Lherzolites and Mantle Processes, Samani, Japan, August 2002.*

Ionov, D. A., Prikhod'ko, V. S. & O'Reilly, S. Y. (1995). Peridotite xenoliths from the Sikhote-Alin, south-eastern Siberia, Russia: trace element signatures of mantle beneath a convergent continental margin. *Chemical Geology* **120**, 275–294.

Ionov, D. A., Bodinier, J.-L., Mukasa, S. B. & Zanetti, A. (2002). Mechanisms and sources of mantle metasomatism: major and trace element compositions of peridotite xenoliths from Spitsbergen in the context of numerical modelling. *Journal of Petrology* **43**, 2219–2259.

Johnson, K. E., Davis, A. M. & Bryndzia, L. T. (1996). Contrasting styles of hydrous metasomatism in the upper mantle: an ion probe investigation. *Geochimica et Cosmochimica Acta* **60**, 1367–1385.

Johnson, K. T. M. (1998). Experimental determination of partition coefficients for rare earth and high-field-strength elements between clinopyroxene, garnet, and basaltic melt at high pressures. *Contributions to Mineralogy and Petrology* **133**, 60–68.

Johnson, K. T. M., Dick, H. J. B. & Shimizu, N. (1990). Melting in the oceanic upper mantle: an ion microprobe study of diopsides in abyssal peridotites. *Journal of Geophysical Research* **95**, 2661–2678.

Kempton, P. D. (1987). Mineralogical and geochemical evidence for differing styles of metasomatism in spinel lherzolite xenoliths: enriched mantle source regions of basalts? In: Menzies, M. A. & Hawkesworth, C. J. (eds) *Mantle Metasomatism*. London: Academic Press, pp. 45–87.

Kent, A. J. R., Stolper, E. M., Francis, D., Woodhead, J., Frei, R. & Eiler, J. (2004). Mantle heterogeneity during the formation of the North Atlantic Tertiary Province: Constraints from trace element and Sr–Nd–Os–O isotope systematics of Baffin Island picrites. *Geochemistry, Geophysics, Geosystems* **5**, paper number 2004GC000743.

Klemme, S., van der Laan, S. R., Foley, S. F. & Günther, D. (1995). Experimentally determined trace and minor element partitioning between clinopyroxene and carbonatite melt under upper mantle conditions. *Earth and Planetary Science Letters* **133**, 439–448.

Kuo, L.-C. & Essene, E. J. (1986). Petrology of spinel harzburgite xenoliths from the Kishb plateau, Saudi Arabia. *Contributions to Mineralogy and Petrology* **93**, 335–346.

McDonough, W. F. & Sun, S.-s. (1995). The composition of the Earth. *Chemical Geology* **120**, 223–253.

McGuire, A. V. (1988a). The mantle beneath the Red Sea margin: xenoliths from western Saudi Arabia. *Tectonophysics* **150**, 101–119.

McGuire, A. V. (1988b). Petrology of mantle xenoliths from Harrat Al Kishb: the mantle beneath western Saudi Arabia. *Journal of Petrology* **29**, 73–92.

Menzies, M. A., Rogers, N., Tindle, A. & Hawkesworth, C. J. (1987). Metasomatic and enrichment processes in lithospheric peridotites, an effect of asthenosphere–lithosphere interaction. In: Menzies, M. A. & Hawkesworth, C. J. (eds) *Mantle Metasomatism*. London: Academic Press, pp. 313–364.

Mooney, W. D., Gettings, M. E., Blank, H. R. & Healy, J. W. (1985). Saudi Arabian seismic deep refraction: a travel-time interpretation of crust and upper mantle structure. *Tectonophysics* **111**, 173–246.

Nasir, S. (1992). The lithosphere beneath the northwestern part of the Arabian plate (Jordan): evidence from xenoliths and geophysics. *Tectonophysics* **201**, 357–370.

Nasir, S. (1995). Mafic lower crustal xenoliths from the northwestern part of the Arabian plate. *European Journal of Mineralogy* **7**, 217–230.

Nasir, S. & Al-Fuqha, H. (1988). Spinel-lherzolite xenoliths from the Aritain volcano, NE-Jordan. *Mineralogy and Petrology* **38**, 127–137.

Nasir, S. & Safarjalani, A. (2000). Lithospheric petrology beneath the northern part of the Arabian plate in Syria: evidence from xenoliths in alkali basalts. *Journal of African Earth Sciences* **30**, 149–168.

Nowell, G. M., Kempton, P. D., Noble, S. R., Fitton, J. G., Saunders, A. D., Mahoney, J. J. & Taylor, R. N. (1998). High precision Hf isotope measurements of MORB and OIB by thermal ionisation mass spectrometry: insights into the depleted mantle. *Chemical Geology* **149**, 211–233.

Shaw, J. E., Baker, J. A., Menzies, M. A., Thirlwall, M. F. & Ibrahim, K. M. (2003). Petrogenesis of the largest intraplate volcanic field on the Arabian plate (Jordan): a mixed lithosphere–asthenosphere source activated by lithospheric extension. *Journal of Petrology* **44**, 1657–1679.

Stein, M. & Goldstein, S. L. (1996). From plume head to continental lithosphere in the Arabian–Nubian shield. *Nature* **382**, 773–778.

Stein, M. & Hofmann, A. W. (1992). Fossil plume head beneath the Arabian lithosphere? *Earth and Planetary Science Letters* **114**, 193–209.

Stein, M., Navon, O. & Kessel, R. (1997). Chromatographic metasomatism of the Arabian–Nubian lithosphere. *Earth and Planetary Science Letters* **152**, 75–91.

Stern, M. & Abdelsalam, M. G. (1998). Formation of juvenile continental crust in the Arabian–Nubian shield: evidence from granitic rocks of the Nakasib suture, NE Sudan. *Geologische Rundschau* **87**, 150–160.

Stern, R. J. & Kröner, A. (1993). Late Precambrian crustal evolution in NE Sudan: isotopic and geochronologic constraints. *Journal of Geology* **101**, 555–574.

Stoeser, D. B. & Camp, V. E. (1985). Pan-African microplate accretion of the Arabian Shield. *Geological Society of America Bulletin* **96**, 817–826.

Thirlwall, M. F. (1991a). High-precision multicollector isotopic analysis of low levels of Nd as oxide. *Chemical Geology* **94**, 13–22.

Thirlwall, M. F. (1991b). Long-term reproducibility of multicollector Sr and Nd isotope ratio analysis. *Chemical Geology* **94**, 85–104.

Turner, S., Hawkesworth, C., Van Calsteren, P., Heath, E., Macdonald, R. & Black, S. (1996). U-series isotopes and destructive plate margin genesis in the Lesser Antilles. *Earth and Planetary Science Letters* **142**, 191–207.

Ulfbeck, D., Baker, J., Waight, T. & Krogstad, E. (2002). Rapid sample digestion by fusion and chemical separation of Hf for isotopic analysis by MC-ICPMS. *Talanta* **59**, 1–9.

Véron, A. J., Church, T. M., Patterson, C. C. & Flegal, A. R. (1994). Use of stable lead isotopes to characterize the sources of

anthropogenic lead in North Atlantic surface waters. *Geochimica et Cosmochimica Acta* **58**, 3199–3206.

Vervoort, J. D. & Blichert-Toft, J. (1999). Evolution of depleted mantle: Hf isotope evidence from juvenile rocks through time. *Geochimica et Cosmochimica Acta* **63**, 533–556.

Volker, F., McCulloch, M. T. & Altherr, R. (1993). Submarine basalts from the Red Sea: New Pb, Sr, and Nd isotopic data. *Geophysical Research Letters* **20**, 927–930.

Whitehouse, M. J., Windley, B. F., Ba-Bttat, M. A. O., Fanning, C. M. & Rex, D. C. (1998). Crustal evolution and terrane correlation in the eastern Arabian Shield, Yemen: geochronological constraints. *Journal of the Geological Society, London* **155**, 281–295.

Windley, B. F., Whitehouse, M. J. & Ba-Bttat, M. A. O. (1996). Early Precambrian gneiss terranes and Pan-African island arc in Yemen: crustal accretion of the eastern Arabian shield. *Geology* **24**, 131–134.

Woolley, A. R. & Kempe, D. R. C. (1989). Carbonatites: nomenclature, average chemical compositions, and element distribution. In: Bell, K. (ed.) *Carbonatites*. London: Unwin Hyman, pp. 1–13.